Contents lists available at ScienceDirect

International Journal of Sediment Research

Original Research

Towards an understanding of southern peri-Pannonian lacustrine depositional cycles: Interplay of sediment delivery and shifting intrabasinal height, a case study of drilled Neogene sediments from northwest Toplica Basin (Central Serbia)

Marija Radisavljević [a], Nikola Burazer [b, *], Aleksandra Šajnović [b], Darko Spahić [c], Gordana Gajica [b], Sabina Kovač [a], Violeta Gajić [a], Branimir Jovančićević [d]

[a] Department of Mining, Crystallography, Petrology and Geochemistry, Faculty of Mining and Geology, University of Belgrade, Belgrade 11000, Serbia
[b] Department of Chemistry, Institute of Chemistry, Technology and Metallurgy, University of Belgrade, Belgrade 11000, Serbia
[c] Department of Regional Geology, Geological Survey of Serbia, Belgrade 11000, Serbia
[d] Department of Applied Chemistry, Faculty of Chemistry, University of Belgrade, Belgrade 11000, Serbia

A B S T R A C T

A multidisciplinary approach allowed the reconstruction of the shallow, highly complex Neogene lacustrine-type sedimentological interplay between the peri-Pannonian (sub)basin subsidence and its seafloor topography. The current study further discusses the mechanism of localized uplift and subsidence by analyzing depositional cycles of middle Miocene sediments drilled in a northwestern or shallower Toplica Basin depocenter (borehole BL4, depth up to 630 m; Central Serbia). Supported by recent constraints on a deeper basinal section of eastern and western subbasin depocenters, the composite study of the segmented Toplica Basin involved geological, sedimentological, mineralogical, inorganic, and organic geochemical analysis, as well as constraints on interchanging geodynamic drivers. The data were extracted from thirty-one selected samples from four sedimentary lithomembers: A, B, C, and D. The architecture of these deposits reflects an intricate pattern influenced by complex lake bottom and subsurface geology (dis)connecting the two depocenters. The investigated Neogene deposition, as a whole, was dominantly controlled by a lithospheric-scale extensional graben system (involving the Jastrebac core complex-type tectonic exhumation) developed on top of the underlying Serbo-Macedonian basement unit. The crustal extension allowed rapid material inflow from other exposed sequences of the juvenile basin, including the abutting surface exposures. During the initial stretching and basin subsidence stage, sediment inflow towards the eastern Toplica depocenter was hindered. The influx of surface-eroded material was interrupted by a natural "obstacle". In turn, such a configuration facilitated voluminous material transport into the western depocenter of the basin, thereby controlling the deposition of lithomembers A and B. After the deposition of lithomember B ceased, the "barrier", or likely intrabasinal structural high, contributed to a reversal of the former westward-directed transport. In that manner, the vertical movements of the structural high enabled material transfer typical for the eastern basin segment, consequently prompting a sedimentary development of the lithomembers C and D.

In this context, mineralogical and geochemical differences between the sequences are used as tracers of depositional changes affected by tectonic events. Sequences of sand and gravel layers of upper lithomembers C and D pointed out that alluvial processes strongly influenced their depositional cycle. On the other hand, a more pronounced presence of sulfide minerals (pyrite concretions) in lithomembers A and B correlated with a calm and anoxic paleoenvironment. The elevated trend of mixed terrigenous and/or microbiologically reworked organic matter (higher carbon/nitrogen (C/N) ratio and terrigenous/aquatic (TAR) ratio, the lower sum of steroids/sum of hopanoids (S/H)) ratio, deposited under anoxic

* Corresponding author.
  E-mail address: nikola.burazer@ihtm.bg.ac.rs (N. Burazer).

—dysoxic freshwater lacustrine conditions (higher pristane/phytane (Pr/Ph) ratio, absence of squalane (i-C_{30}) and β-carotene), is observed towards a shallower section of the borehole (lithomembers C and D).

1. Introduction

The intriguing dynamics of depositional processes, e.g., an interplay with rapidly interchanging tectonic movements in lacustrine environments, remains one of geochemistry's most puzzling problems (Balázs et al., 2018; Cohen, 2003; Fornari et al., 2001; Harzhauser & Mandić, 2008; Lone et al., 2018; Mandić et al., 2019b; 2019c; Marić et al., 2019a; Meyers & Ishiwatari, 1993, Meyers & Lallier-Vergès, 1999; Obradović & Vasić, 2007; Scott et al., 2012; Vlček et al., 2020, 2022). The sensitivity lies in lakes' complexity in terms of the delicate interplay between physical or spatial (e.g., the bathymetry of paleolakes and tectonics; Balázs et al., 2018), chemical, and biological properties. Regarding the specific research objectives, a multidisciplinary approach involving geology, sedimentology, mineralogy, geochemistry, geodynamics, etc., represents a promising way to decipher the nature of these changes affecting the basin-scale sedimentological process (e.g., Cohen, 2003; Mandić et al., 2019a, 2019b; Rybár et al., 2015, 2016).

Crustal-scale tectonic activity, the inception and formation of extensional faults (e.g., Rybár & Kotulová, 2023; Spahić et al., 2011, 2013; Subová et al., 2022; Tari et al., 2021), asymmetric subsidence (e.g., Balázs et al., 2021), developing volcanism (Lukács et al., 2018, 2022), and paleo-alluvial processes (alluvial fans, e.g., Budai et al., 2019), including diverse paleoenvironmental, paleoclimatic, and lake level fluctuations (Harzhauser & Mandić, 2008; Katz & Lin, 2014; Kováč et al., 2018; Lone et al., 2018; Mandić et al., 2011; 2019a; Marović et al., 2002; Meyers & Ishiwatari, 1993, Meyers & Lallier-Vergès, 1999; Nováková et al., 2020; Orkhonselenge et al., 2022; Pezelj et al., 2013; Sant et al., 2020) appear to be "driving forces" controlling sedimentary deposition in basins (Allen & Allen, 2013). The influence of several geogenic factors on deep, shallow marine, and, in particular, lacustrine deposition or associated stratigraphic patterns, is reflected by the changes in sediment delivery and associated sequences (lithological content, mineralogical distribution, heavy mineral composition, e.g., Frihy et al., 2022), content of major/trace elements, and an eventual presence of biomarker signatures (Budai et al., 2019; Burazer et al., 2020; Vlček et al., 2020, 2022). For instance, the presence of volcanoclastic fragments in sediments may suggest that volcanic eruptions or erosion/weathering of emerging volcanic rocks have occurred in the vicinity of the investigated basin (e.g., Jordan et al., 2022; Sandiford et al., 2001; Šarinová et al., 2018, 2021a, 2021b). These igneous fragments can either be mafic (amphibole, pyroxene, biotite, etc.) or felsic type (quartz, K-feldspar, plagioclase, etc.). Subaerial exposure, fluvial or eolian processes are the weathering means producing denudation and sediment transport of eroded igneous material (Orkhonselenge et al., 2022; Valero-Garcés et al., 2014). Importantly, volcanic presence or paleo-volcanic activity in the basin may propagate their ability to elevate underlying crustal paleo-heat flows. Variations in basement paleo-heat flow values may lead to significant intra-formational (paleo)temperature changes (e.g., Balázs et al., 2021; Hakimi et al., 2018; Peshkov et al., 2021), inducing the alteration of biomarkers, often used as indicators of the maturity evolution of organic matter (OM) deposited in sediment (e.g., Allen & Allen, 2013; Burazer et al., 2020).

Weathering, paleo-alluvial processes, extensional exhumation, and the inversion of tectonic subsidence may be responsible for sediment exposure to terrestrial conditions, allowing further erosion and sediment influx. Such a process is frequently sourced by exhumed basinal rocks and their emerging sections. Eroded rock sections, i.e., eroded material, can be redeposited in sedimentary basins, accounting for a renewed extension and subsidence episode. In such cases, sediments may contain a complex mixture of indistinctive yet articulated environments providing valuable information capable of describing the paleoenvironmental settings attached to different depositional cycles, i.e., their deposition and superimposition (Burazer et al., 2021; Nováková et al., 2020).

In the lithological context, alluvial deposits of the wider Pannonian area are usually characterized by unconsolidated sand and gravel layers, often with residual OM particles (Budai et al., 2019; Burazer et al., 2021; Gaigalas et al., 2013; Giraudi, 2014; Vlček et al., 2020, 2022). Once transported into a subaqueous basin environment, preservation and accumulation of the OM in sedimentary basins depend on a variety of environmental factors, in particular, redox conditions and salinity (Burazer et al., 2020; Didyk et al., 1978; Grice et al., 1998; Jiamo et al., 1990; Jiang & Fowler, 1986; Katz & Lin, 2014; Sinninghe Damasté et al., 1995). Anoxic and saline paleoenvironmental conditions, marked by highly abundant phytane, regular isoprenoid i-C_{25}, and β-carotene, favor the accumulation and preservation of the OM in the sediment (Didyk et al., 1978; Grba et al., 2014; Grice et al., 1998; Jiamo et al., 1990; Jiang & Fowler, 1986; Sinninghe Damasté et al., 1995). It is worth mentioning that volcanic ash often provides nutrients and metal ions, stimulating the proliferation of algae/bacteria and thereby enhancing the primary productivity itself (Duggen et al., 2007; Nováková et al., 2020; Olgun et al., 2013; Uematsu et al., 2004; Vlček et al., 2020, 2022).

The study area covers middle Miocene buried sediments extracted as four lithomembers from fully cored borehole BL4, which is positioned between the eastern and western subsegments of the Neogene Toplica Basin (Central Serbia, southern peri-Pannonian realm; Figs. 1(a)–1(c)). The investigated depositional cycles reflect the relation between accommodation space, sediment supply, and seafloor topography, causing their localization and abrupt changes in sediment distribution patterns (depicted in borehole BL4). The emerging seafloor topographic feature (or the "ramp") seems to have an essential role in the sediment supply of the investigated lithomembers. The main goal of the current study is to elucidate the interplay between the basin subsidence and its seafloor topography, the tectonic uplift mechanism, and the nature of depositional cycles. A multidisciplinary approach was applied to examine the abrupt changes and transitions in the material inflow patterns from the (i) uplifted surface-emerging basinal segments and (ii) abutting marginal parts of the Toplica Basin (may also include exposed basement fragments). To understand the nature of the abrupt changes in sediment distribution patterns, the following composite study is somewhat connected to previous investigations, which provided the constraints on Prebreza and Čučale sediments (northwestern, BL7, and central BL5 and BL3 segments of the Toplica Basin; Burazer et al., 2020, 2021).

2. Geological settings and tectonic background of the Neogene Toplica Basin

The Toplica Basin is a smaller satellite basin (Bartha et al., 2022) located in the southern segment of the Pannonian Basin in Central Serbia, occupying about 200 km² (Figs. 1(a) and 1(b)). This is a morphologically well-marked neostructural feature accommodated between mountain massifs in proximity to the Jastrebac Mountain in the north (Divljan, 1979; Marović, Đoković, Toljić, Milivojević et al., 2007a; Spahić, 2006), having the Kopaonik Mountain in the west, and Pasjača and Vidojevica Mountains in the southeast. On its eastern margin, the Toplica Basin is connected with a Niško-Dobrički Neogene Basin (Fig. 1(c)). The Toplica Basin is mainly filled with Neogene sediments deposited on top of the much older underlying Serbo-Macedonian gneisses (Antić et al., 2016). The Toplica Basin is a tectonically landlocked Neogene basin surrounded by a Paleogene granodiorite on the north, Jurassic diabase, gabbro, serpentinized peridotite, serpentinite, ophiolitic mélange, and Paleozoic phyllite on the west, Precambrian micaschist, gneiss, Upper Cretaceous flysch, and Neogene volcanic breccia, tuff, andesite on the northeast and east (Erak et al., 2017; Marović et al., 2007c; Fig. 1(c)). The Toplica Basin, or Toplica graben having an E—W elongated shape is a result of diverse lacustrine sedimentary environments characterized by rapid subsidence (Dimitrijević, 2000; Malešević et al., 1974; Obradović & Vasić, 2007; Spahić et al., 2023).

2.1. Neogene formations of the Toplica Basin

Recent studies by Burazer et al. (2020, 2021) offer geological, mineralogical, petrological, and geochemical insight into the lower—middle Miocene Čučale and Prebreza lacustrine sediments in the Toplica Basin. These sedimentary formations were deposited in the western and eastern segments or mini-depositional centers of the Toplica Basin (Fig. 1(c)). The onset of Neogene deposition commenced with fine-grained Čučale clastites of the Lower Miocene age, interrupted by a hiatus (Burazer et al., 2020) succeeded by fine-, medium- and coarse-grained Prebreza clastites deposited during the middle Miocene. The influx of medium- and coarse-grained Prebreza clastites indicative of abrasion of abutting marginal parts represents a terminal basin filling stage of this paleo-lake. In that manner, the Prebreza unit is marking a slow infill, providing conditions for a gradual basin closure that lasted until the end of the middle Miocene (Burazer et al., 2020).

A significant presence of volcano clastites in the form of analcimized tuffs, tuffites, and other tuffaceous types is documented in Prebreza and Čučale sediments (borehole BL7, Fig. 1(c)). The presence of volcanic derivatives suggests that the intense volcanism has followed a primary depositional cycle in this compartment of the Toplica Basin (Burazer et al., 2020). Prebreza sediments are enriched in algal OM deposited in anoxic and hypersaline-to-mesosaline conditions. In contrast, mixed microbiologically reworked/terrestrial OM deposited in mesosaline to freshwater settings are consistent with the deposition of Čučale sediments. Volcanic ash and the release of its nutrients/metal ions in lake water have undoubtedly promoted algae/bacteria proliferation, leading to hydrocarbon formation. Hydrocarbons are observed within the upper part of the Čučale unit (Burazer et al., 2020).

Opposite to the western (mini)depocenter, deposition and accumulation of the eastern basinal sequences (boreholes BL3 and BL5, Fig. 1(c)) were strongly influenced by alluvial-lacustrine processes (Burazer et al., 2021). The onset of the depositional cycle of the Prebreza and Čučale formations in this secondary depocenter is consistent with an inflow of eroded older sedimentary rocks (not abutting basement metamorphic rocks). The exposed basinal section and eroded material were transported by river flows, yielding a mixture of older and younger sedimentary rocks. The mixture of different rock sources brought into the basin contains complex information about the OM type and the prevailing syndepositional paleoenvironmental conditions. Generally, a terrigenous type of OM in the Prebreza and Čučale units was deposited under warm and semi-humid/semi-arid to semi-humid climate periods, characterized by a marginal presence of algal biomass (observed in some Čučale sediments and the lower parts of Prebreza unit; Burazer et al., 2020). Taking into consideration the previous reports, as well as the position of borehole BL4 itself (Fig. 1(c)), it appears that the geology of the investigated borehole section depicts a kind of "barrier" (likely an intrabasinal structural high, allowing/preventing a sedimentary communication between the eastern and western depocenters of the Toplica Basin).

3. Samples and analytical methods

3.1. Samples

The current study represents a well-based multiproxy composite survey and includes a conventional regional geological approach. The composite sedimentological-stratigraphic-organic geochemistry study is accomplished by analyzing thirty-one selected core samples collected and extracted from borehole BL4 (depth 630 m, Table 1, Fig. 2). A pestle and mortar were used for pulverizing the samples. Granulometric, optical analysis, complexometric determination of calcium and magnesium contents, X-ray powder diffraction (XRPD), Scanning Electron Microscopy (SEM), X-ray fluorescence (XRF), elemental analysis, and Soxhlet extraction methods were used for the selected samples. Before doing XRF and elemental analysis, the samples were dried at 105 °C in a humidity chamber, whereas optical examination, SEM, XRPD, and Soxhlet extraction methods did not require a drying step.

3.2. Optical analysis

Selected samples of bound, semi-bound, and unbound sedimentary rocks and sediments were optically examined. The analysis was done using a LEICA DMLSP polarized transmitted light microscope connected to a LEICA DFC290HD camera via the LAS V4.1 program (Leica Microsystems, Wetzlar, Germany) and a LEICA EZ4D binocular magnifier.

3.3. Scanning electron microscope with an energy-dispersive spectrometer (SEM-EDS)

Scanning electron microscopy is used on the selected samples by applying a JEOL JSM-6610LV electron microscope connected to an X-Max Large Area Analytical Silicon Drift energy-dispersive spectrometer (Oxford) working in high vacuum conditions. Images of the samples were obtained using secondary electron (SEI) and backscattered electron (BSE) detector shaving a tungsten filament as the electron source. For this method, the samples should not have a cover glass and must be electrically conductive. The surfaces of the polished pieces were previously vaporized with a conductive layer of carbon or gold on a vaporizer type BALTEC-SCD-005. The process was done with an operating voltage of 20 kV. An energy-dispersive spectrometer using internal and external standards was used for chemical analyses. The internal standards are software-defined. Al-albite, Na-albite, Si-albite, K-orthoclase, Mg-diopside, Fe-standard of metallic iron, Ca-wollastonite, Cr-chromium oxide, Ti-rutile, Mn-standard of metallic iron, elemental manganese (Mg), S-pyrite, Cl-halite, Zr-zircon, P-apatite were used as external standards (where Al is aluminum, Na is sodium, Si is
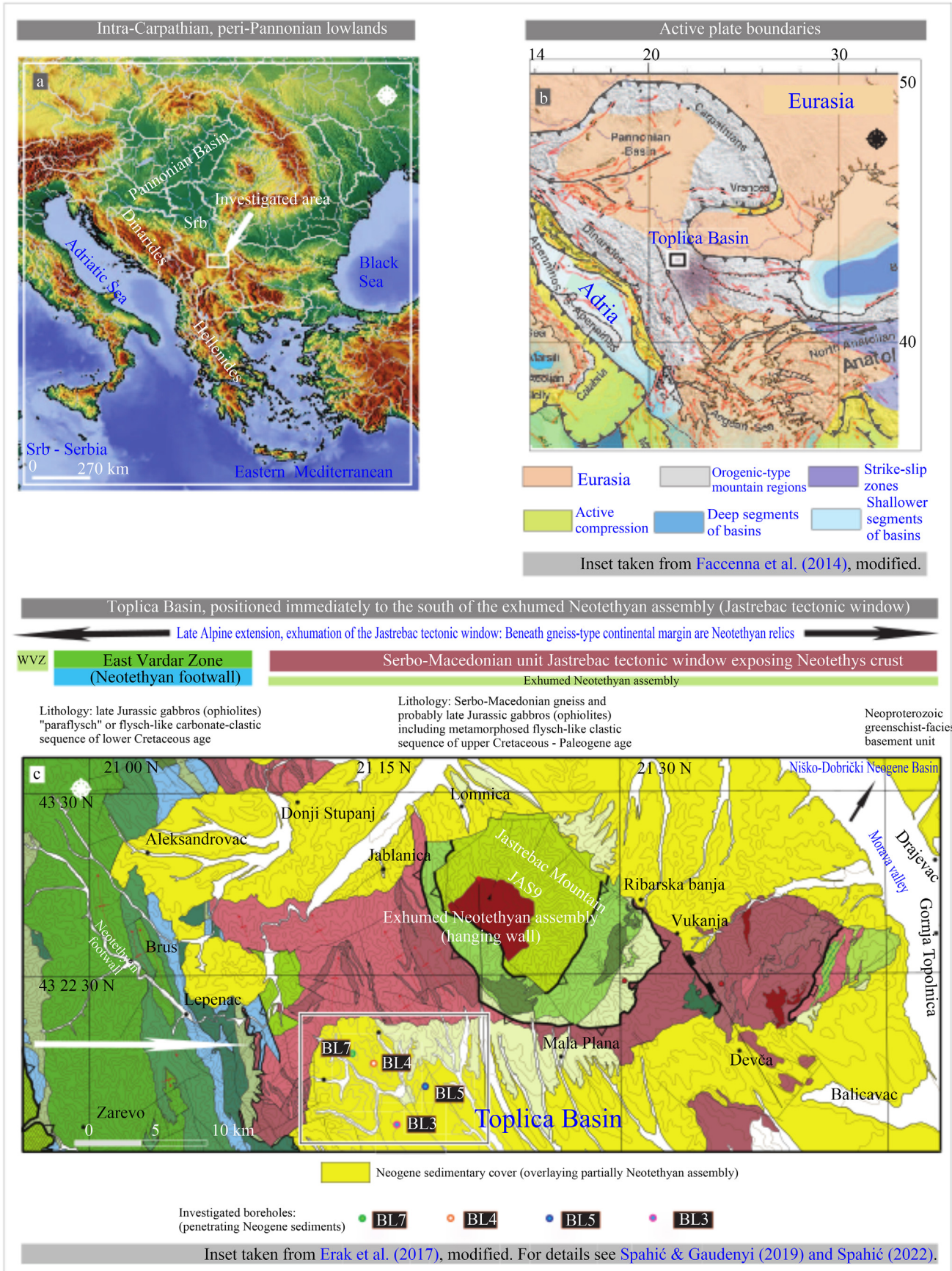
Inset taken from Faccenna et al. (2014), modified.

Inset taken from Erak et al. (2017), modified. For details see Spahić & Gaudenyi (2019) and Spahić (2022).

Table 1
Samples list, lithofacies, lithomembers, and depth of investigated samples from borehole BL4.

Lithofacies	Lithomembers	Sample	Depth (m)
Alluvial-lacustrine	/	BL4/1	15
		BL4/2	20
		BL4/3	37
		BL4/4	42
Lacustrine	D	BL4/5	65
	C	BL4/6	79
	D	BL4/7	106
	C	BL4/8	118
		BL4/9	138
	D	BL4/10	160
		BL4/11	193
		BL4/12	213
	C	BL4/13	246
		BL4/14	274
		BL4/15	278
	A	BL4/16	302
		BL4/17	321
		BL4/18	332
		BL4/19	365
	B	BL4/20	375
	A	BL4/21	391
	B	BL4/22	413
	A	BL4/23	445
	B	BL4/24	458
	A	BL4/25	480
		BL4/26	496
		BL4/27	521
		BL4/28	541
		BL4/29	561
		BL4/30	578
		BL4/31	606

silicon, K is potassium, Mg is magnesium, Fe is iron, Ca is calcium, Cr is chromium, Ti is titanium, Mn is manganese, S is sulfur, Cl is chloride, Zr is zirconium, and P is phosphorus). The results are represented as a sum of the contents of elements given in mass (mass%) and atomic (at.%) percentages, later normalized to 100%. The detection limit of the element contents is about 0.1 weight (wt %) percent, meaning that if an element is absent in the analyte, the concentration of the element may be below 0.1 wt%. The contents of light elements (with atomic numbers 1–5, i.e., from hydrogen (H) to boron (B)) were not measured because this method cannot detect elements with these atomic numbers.

3.4. Granulometric analysis

Loose and friable samples (Table 2) were subjected to granulometric analysis. The samples were separated by a wet sieving method according to the predefined fractions (500–63 μm). Afterward, samples were dried and measured. Since only two samples from the borehole corresponded to loose-type sediments, results are presented exclusively for these two samples belonging to the alluvial-lacustrine facies. Tests were done under a binocular magnifying glass or a polarizing microscope in an immersion liquid (xylene).

3.5. X-ray powder diffraction (XRPD)

The X-ray powder diffraction experiment was done using a Rigaku SmartLab X-ray diffractometer in $\theta-\theta$ geometry (samples in horizontal position) in a parafocusing Bragg−Brentano geometry on selected samples (Figs. 3 and 4). A strip detector D/teX Ultra 250 in one-dimensional (1D) standard mode with copper $(Cu)K\alpha_{1,2}$ radiation source ($U = 40$ kV and $I = 30$ mA) was used. The XRPD patterns were collected in the 3°−70° 2θ range (2°−30° 2θ for clay minerals), with a step of 0.01° and a data collection speed of 10° per min with horizontal sample rotation of 30 rpm. Each sample was prepared in a standard sample holder. PDXL 2 software (Version 2.8.3.0. Rigaku Corporation, Tokyo, Japan, 2007) was used for the powder diffraction data analysis. For a closer definition of layered silicate minerals, especially clay minerals, samples were prepared using a particular procedure. Well-oriented clay minerals were prepared from the aqueous suspension on glass plates, which were air-dried and then saturated in a chosen medium with ethylene glycol (EG) thermally treated at 550 °C. Prepared sample slides were tested under the stated conditions and in the predicted range to characterize clay minerals.

3.6. X-ray fluorescence (XRF)

The Retsch PP25 hydraulic press was used to prepare chosen samples as pressed pellets. The process required mixing the investigated sediment and tableting aid wax in a ratio of 85:15. Selected samples were subjected to semi-quantitative and qualitative analyses using an ARL PERFORM'X Sequential X-Ray Fluorescence Spectrometer (Thermo Fisher Scientific, Switzerland). Stream-type sediment (STSD-3, 1990) was used as a standard for this analysis. The spectrometer equipment included a 4200 W Rh X-ray tube, goniometer, seven optical crystals (AX03, AX09, AX16C, PET, GE111, LiF200, and LiF220), and two detectors (flow proportional counter—FPC and scintillation detector—SC). ARL software UniQuant, specialized for standardless analysis, was applied for semi-quantitative analysis. In contrast, qualitative analysis was done to eliminate any doubts about measurements of elements close to the detection limit, and unlikely interferences emerged because of the line overlaps (OXSAS, 2013; UniQuant, 2015).

3.7. Elemental analysis

To eliminate carbonates, the selected samples were pre-treated with diluted hydrochloric acid (HCl, 1:3, volume:volume (v:v)). The elemental analysis of carbon (C), hydrogen (H), nitrogen (N), and sulfur (S) was done using a Vario EL III, CHNS/O Elemental Analyzer, Elementar Analysensystem GmbH, with the application of coal as a standard (NCS FC 28009L, 2016).

3.8. Complexometric determination of calcium and magnesium

The complexometric method involves the destruction of the selected samples with 36% HCl. Subsequently, the contents of Ca^{2+} and Mg^{2+} were determined by titration with a complexone (ethylenediaminetetraacetic acid—EDTA) solution and a buffer solution. Titration indicators were murexide for Ca^{2+} and eriochrome black T for Mg^{2+}, whereas the buffer solution used during titration was ammonium chloride/ammonium hydroxide (NH_4Cl/NH_4OH). A 0.01 M complex one solution (prepared for this method) reacted with Ca^{2+} and Mg^{2+} ions in a 1:1 M ratio. Calculations provided the amount of calcium oxide (CaO) and magnesium oxide (MgO) corresponding to the sample's calcite and dolomite contents.

Fig. 1. (a) A relief map exposing the investigated peri-Pannonian Toplica Basin, (b) main tectonic units and fault zones engulfing the Pannonian Basin, including the position of the Toplica Basin (Facenna et al., 2014, modified), (c) location of the Toplica Basin, including four exploration wells within the Jastrebac core-complex (inset modified after Erak et al., 2017). The Jastrebac core-complex represents the NeoTethyan Vardar pre-Neogene complex. Neogene veneer, including the explored segment of Toplica Basin, is at the southeastern side of the Jastrebac Mountain complex.
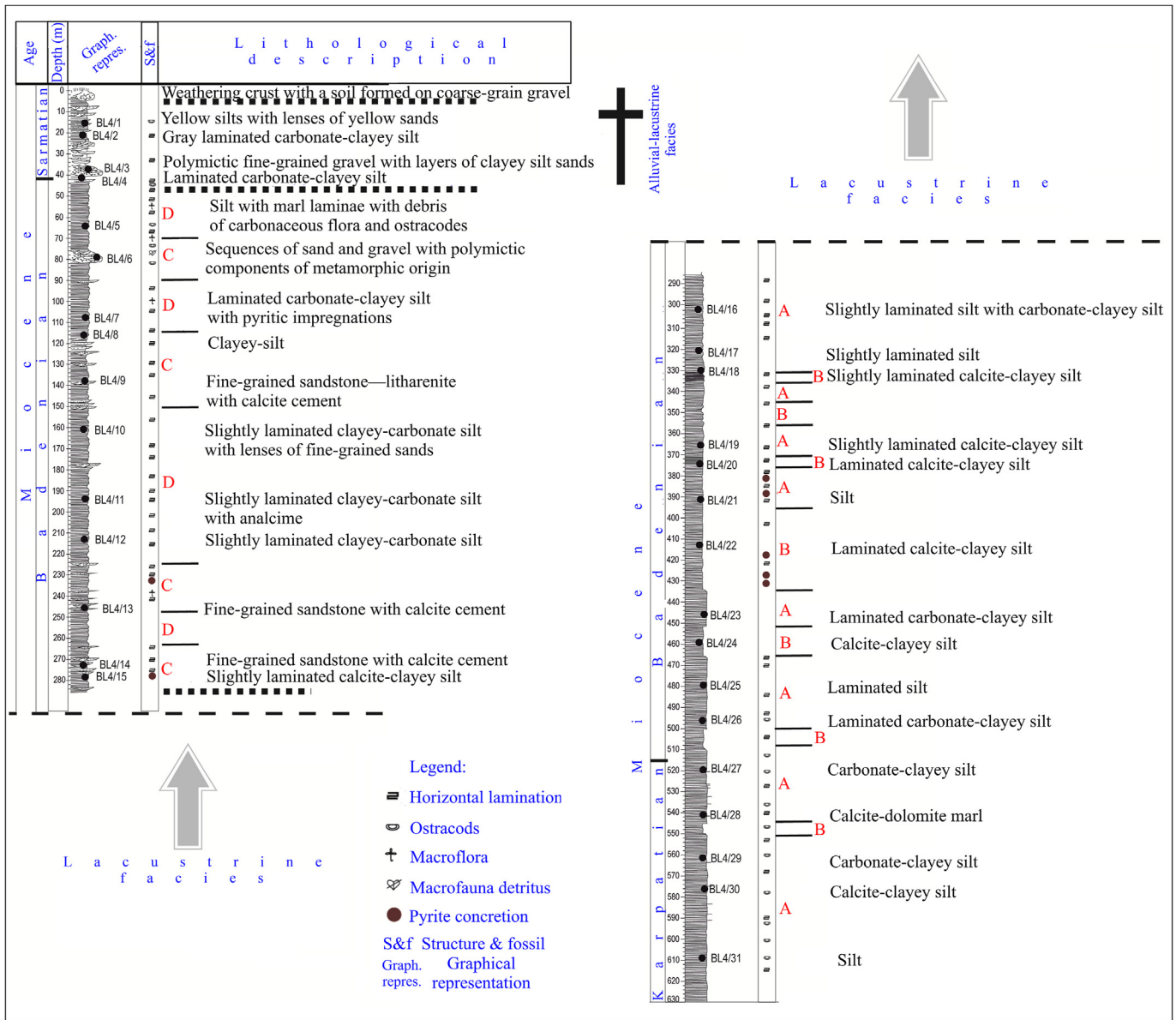
Fig. 2. Lithostratigraphic column of borehole BL4.

Table 2
Granulometric composition of sands from borehole BL4.

Fraction (f) size	BL4/1	BL4/3
	(%)	
>0.5 mm Coarse sand and gravel	/	0.17
0.5−0.25 mm Medium sand	0.54	27.28
0.25−0.125 mm Fine sand	34.23	55.45
0.125−0.063 mm very fine sand	42.29	4.47
<0.063 mm Slit and clay	22.94	12.63
Sorting properties	1.434 (Well-sorted)	1.330 (Well-sorted)
Average grain size	0.117 mm	0.218 mm
Standard deviation	1.006	1.044

3.9. Organic geochemical analysis

Azeotrope mixture of methanol and dichloromethane (1:7.6, v:v) was used for the Soxhlet extraction of selected samples, which lasted approximately 36 h. Elemental sulfur was removed by adding copper to the mixture. Only the saturated fraction was isolated from bitumen using column chromatography (adsorbents: silicon dioxide (SiO_2) and aluminum oxide (Al_2O_3), eluent: *n*-hexane). Subsequently, the saturated fraction was analyzed on an Agilent 7890A GC gas chromatograph coupled to an Agilent 5975C mass selective detector. The column was heated from 80 to 300 °C at a rate of 2 °C/min, and the temperature of 300 °C was maintained for an additional 20 min. Subsequently, the temperature of 300 °C was rapidly increased to 310 °C, at a rate of 10 °C/min, whereas the final
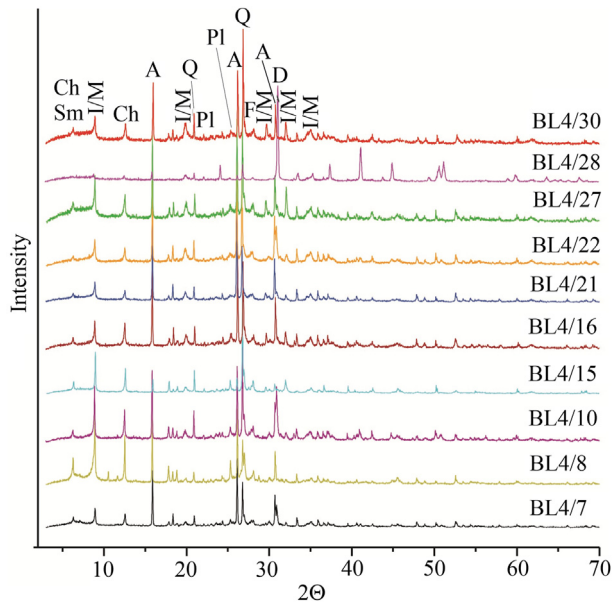
Fig. 3. X-ray diffractograms of selected samples from lithomembers A, B, C, and D: BL4/7 and BL4/10 (lithomember D); BL4/8 and BL4/15 (lithomember C); BL4/22 (lithomember B); and BL4/16, BL4/21, BL4/27, BL4/28, and BL4/30 (lithomember A). Sm—smectite, Ch—chlorite, I/M—illite/muscovite, A—analcime, Q—quartz, Pl—plagioclase, F—K-feldspar, and D—dolomite.

temperature of 310 °C was maintained for 1 min. Mass fragmentograms of the saturated fraction used for the interpretation of biomarkers were m/z 71 for n-alkanes and isoprenoids, m/z 125 for β-carotane, m/z 215 and m/z 217 for steroids, and m/z 191 for terpenoids.

4. Results

4.1. Lithological description of the Neogene sequences

The Toplica sedimentary pile as a whole consists exclusively of Neogene sediments overlain by Quaternary unconsolidated deposits (Fig. S1 in the Electronic Supplementary Material (ESM)). The investigated Neogene sediments were collected from borehole BL4, located between the eastern and western subsegments of the basin (Fig. 1(c)). Constraints on the petrological composition, structural characteristics, and biostratigraphy have provided valuable insight into the lake's lithological and paleoenvironmental settings (Burazer et al., 2020, 2021; Fig. 2). The new data have indicated the deposition of the two principal syn- and post-rift facies: alluvial-lacustrine (0—40 m) and lacustrine (40—630 m, Fig. 2). The investigated lacustrine facies can further be characterized by a lithological and structural diversity, described in the following lacustrine lithomembers or facies: A, B, C, and D (Fig. 2):

(i) Lithomember A is a dominant sequence, with the layer thicknesses reaching up to 80 m. This sedimentary series consists of fine-grained loose clastites or pelites with particles smaller than 0.05 mm. The main structural feature is horizontal lamination, which can be more or less pronounced. In addition to quartz, feldspar, mica, and clay minerals, carbonates (calcite and dolomite), volcaniclastic material, and a sandy fraction are documented as secondary petrogenic components. Siltstone, claystone, marl, and other rocks are the main lithotypes formed by combining the main petrogenic components. Analcime is a consistent mineral documented across the entire depositional cycle. The presence of OM is higher compared to lithomember B. Several samples in the lower part of the drilled column likely contain
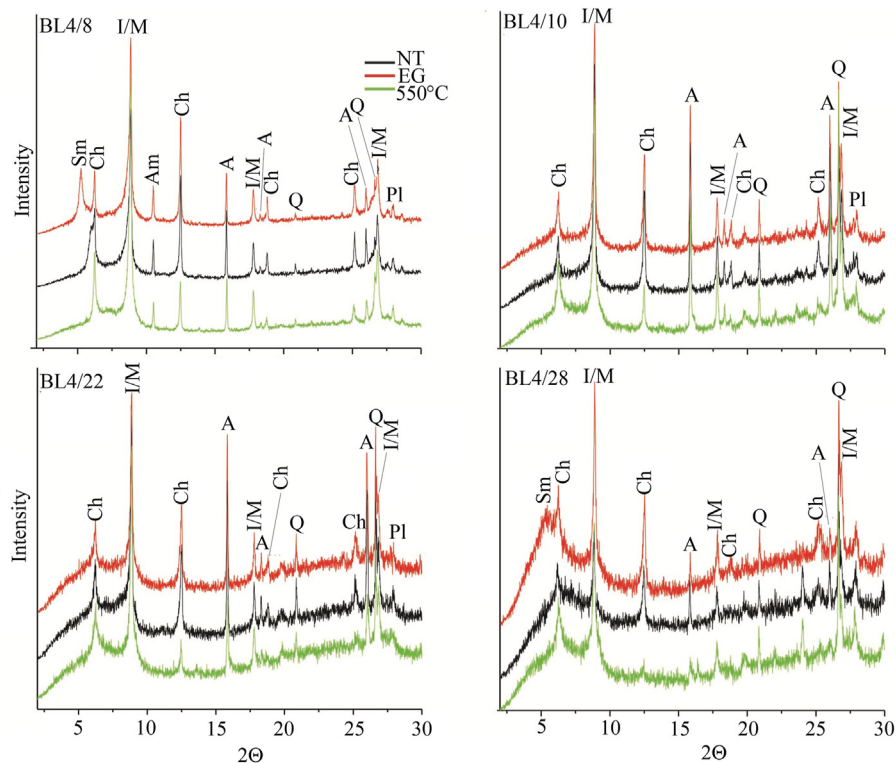

Fig. 4. X-ray diffractograms for oriented samples with and without the presence of smectite: BL4/8 (lithomember C), BL4/10 (lithomember D), BL4/22 (lithomember B), and BL4/28 (lithomember A). NT—Non-treated samples, EG—samples treated with ethylene glycol, 550 °C—samples heated at 550°C, Sm—smectite, Ch—chlorite, I/M—illite/muscovite, Am—amphibole, A—analcime, Q—quartz, and Pl—plagioclase.

older ostracod shells (Fig. 5(a)). Various sulfide and siliceous-type concretions are classified as secondary chemical structural forms. Sulfide concretions have the form of fresh or oxidized sulfides, such as pyrite having a raspberry-like morphology (pyrite framboids, Fig. 5(b)). The observed fractures are extensional joints filled with sulfides, carbonates, or bitumen (Fig. 5(c)).

(ii) Lithomember B is defined as Laminites since the lithomember is characterized by extraordinarily well-developed horizontal lamination (Fig. 5(d)). The observed thin laminae have different colors, compositions, and structural characteristics. Fine-grained clastites with a slightly higher content of the OM and sulfides are present. The lithomember comprises fine-grained clastites with quartz, feldspar, mica, and carbonates (calcite and dolomite), including clay minerals and products of transformed volcanic material and sulfides. The observed laminae consist of siltstone, claystone, and marlstone, further exposing complete sedimentary transitions. The observed lamination is a synsedimentary texture, indicating the presence of the structural forms typical for post-sedimentary stages. The laminations mapped are wavy lamination, convolution, stretching, and opening, which were active during the extension. The appearance of this lithomember is consistent with deeper levels of the Neogene lacustrine facies.

(iii) Stratigraphically, lithomember C is the lowermost and oldest fine-grained clastic sequence containing thin layers or lenses of fine-grained sandstones. The thickness of lithomember C varies from a few meters reaching tens of meters. Lithomember C is consistent with the upper part of the paleo-lake substrate, starting from 285 m in depth (towards the bottom of the well). Fine-grained clastites consist of quartz, feldspar, mica, clay minerals, carbonates (calcite and dolomite), and analcime. A dominant rock type is siltstone, enriched with laminae having sandy, marly, or tuffaceous character. Sandstones in thin layers or lenses have fine-grained structures consisting of quartz, feldspar, and other rock fragments. Mapped fragments comprise schists, mica schists, quartzites, and older carbonate rocks, with muscovite, biotite, and chlorite minerals emplaced into a clayey matrix or calcite cement. Sandstones are consistent with subarkoses, subordinately subliteranites. Dominant structural forms are horizontal and cross-lamination. At the same time, gradation can be observed in the sandstone layers or
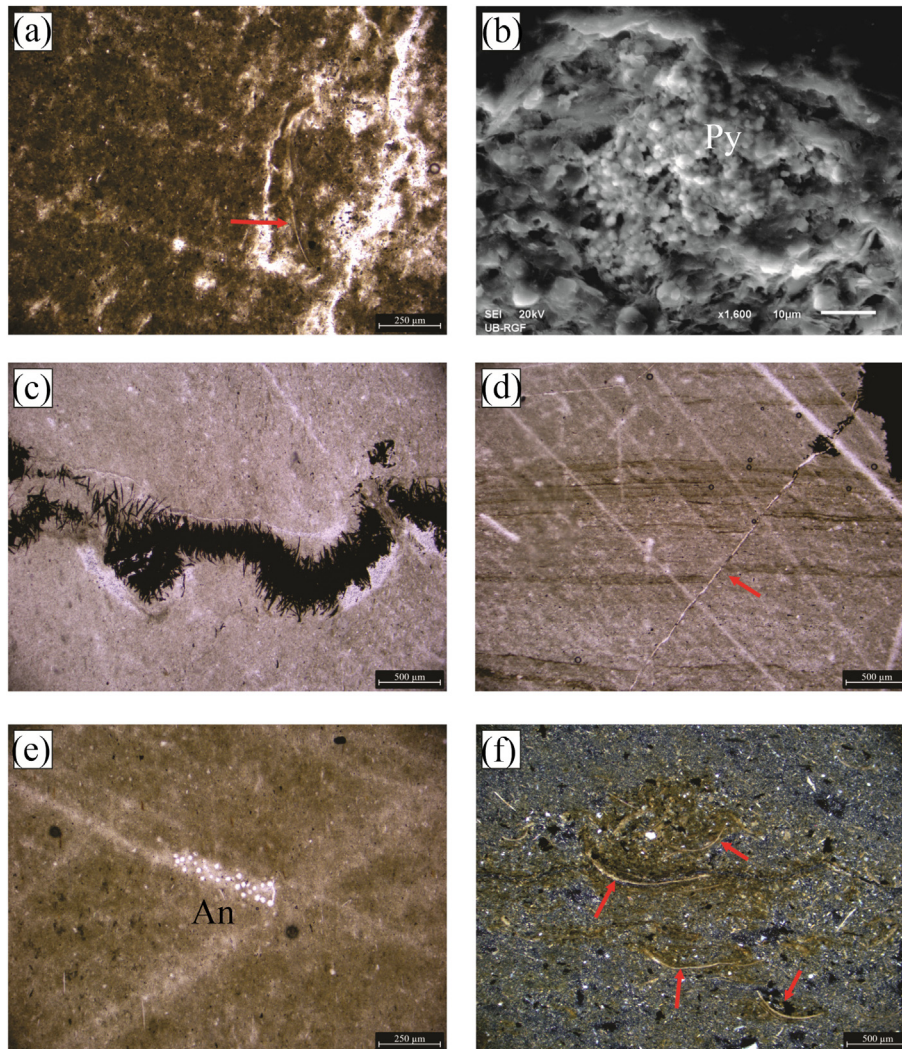

Fig. 5. Photomicrographs of selected samples: (a) remains of ostracod macrofauna (marked with the red arrow), most likely redeposited in the lowest parts of the lithological column (BL4/31), (b) framboidal pyrite, Py (BL4/29), (c) the cracks represented the predisposed directions along which needle-like accumulations of iron sulfide (Py) were formed (BL4/19), (d) fine-grained siltstones of lithomember B with horizontal lamination and microfault marked with the red arrow (BL4/22). (e) Weakly laminated argillaceous siltstone with analcime (An) accumulations (BL4/11), and (f) fossil remains (marked with red arrows) of ostracods and carbonaceous flora in alluvial-lacustrine facies (BL4/4).

bodies, indicating a granulometric differentiation typical for lower-density suspensions. Pyrite concretions belong to secondary structural forms.

(iv) Lithomember D is similar and consistent with fine-grained clastites comprising quartz, feldspar, and mica. It consists primarily of siltstones (Fig. 5(e)), with a certain amount of clay and carbonate components, whereas siltstone, marlstone, and clayey laminae alternate. Additionally, it has a considerably pronounced lamination consistent with a primary structure, whereas a cluster of pyritic concretions appears as the secondary structure. The fossil remains of ostracods and carbonaceous flora debris represent the organogenic component (Fig. 2).

After the lacustrine deposition ceased, the Toplica Basin infill continued, reaching nearly 40 m of thick alluvial-lacustrine sediments (Fig. 2). Thick alluvial-lacustrine sediments are organized in the foregoing sequences with the mapped changes of thickness having the sets grading upwards (towards the Earth's surface). The uplift and exposure to erosional processes have significantly reduced the original emerging sedimentary layer thickness. At an almost identical time, a few erosional episodes are recorded in the eastern depocenter, succeeded by a development of the paleosols (Burazer et al., 2021). In terms of composition, fine-grained gravel and siltstones with clayey, sandy, and carbonate components are dominant. There are several varieties and transitions towards clayey and sandy siltstones containing a carbonate component. The dominant structural feature is horizontal lamination. A notable presence of redeposited metamorphic rock fragments suggests that the material accumulating in the basin was transported from its northern margin (Jastrebac Mountain, Fig. 1(c)). The occurrence of redeposited fragments of ostracod shells also follows the alluvial-lacustrine sequence (Fig. 5(f)). The sands and sandstones that occur in the upper part of the unit have significant similarities, however, with a slightly higher proportion of redeposited rock fragments. The presence of medium- and coarse-grained clastites illustrates a terminal lake stage and a slow closure of the entire Toplica Basin.

4.2. Mineralogical composition

4.2.1. Alluvial-lacustrine facies

The optical examination of sands (BL4/1 and BL4/3) has been done for all fractions (f) except for $f < 0.063$ mm. The samples are interpreted as well-sorted, fine-grained sands, whereas sample BL4/1 can be characterized as siltstone. The most abundant constituents are quartz (including quartzite), rock fragments, feldspars, and coated grains. Other components are minerals with contents less than 1%, namely carbonates, phyllosilicates (muscovite, biotite, chlorite), and heavy minerals (Table 3). Petrogenic constituents were coated with iron oxides, and hydroxides or carbonates, for which closer determination is impossible, are separated into a category called coated grains. Heavy minerals, whose presence is higher in sample BL4/3, expose biotite (dominantly in BL4/1), metallic minerals, and rock fragments (mostly in BL4/3), with a subordinate presence of epidote, hornblende, apatite, garnet, chlorite, and alusite, staurolite, coesite, calcite, sphene, tourmaline, rutile, and pyroxene.

4.2.2. Lacustrine facies

Table 4 and Figs. 3, 4, and 6 demonstrate the mineral distribution in investigated facies obtained via SEM-EDS and XRD. Generally, the investigated sequences are characterized by a higher presence of quartz (SiO_2), having irregularly shaped grains, mostly rounded ones. Quartz predominates over other minerals in

Table 3
Modal analyses of sands from borehole BL4.

Minerals in %	Sands	
	BL4/1	BL4/3
Quartz	19.44	41.77
Feldspar	1.69	5.08
Rock fragments	74.01	34.62
Calcite	0.98	1.11
Muscovite	0.26	0.17
Biotite	0.96	0.14
Chlorite	0.07	0.05
Coated minerals	2.29	14.53
Heavy minerals	0.31	2.54

lithomember C, particularly in sandstones of samples BL4/9 and BL4/14 (Table 4, Fig. 6(a) and 6(c)). The grain size of quartz in the sandstones has variations, ranging from a maximum of 0.15 mm × 0.2 mm down to a very small size of 10 μm × 10 μm, consistent with siltstones.

In addition to quartz, the principal mineral phase (Table 4, Figs. 3, 4, and 6) comprises K-feldspar ($KAlSi_3O_8$), dolomite ($CaMg(CO_3)_2$), calcite ($CaCO_3$), plagioclase ($(Na,Ca)Al_{1-2}Si_{2-3}O_8$), and analcime ($Na(AlSi_2O_6) \cdot H_2O$). K-feldspar is particularly well observed in lithomember C (BL4/9 and BL4/14), whereas carbonate minerals, calcite, and dolomite are abundant in lithomembers C and A, prominently in member A (BL4/28, Table 4). The grain size of dolomite in sample BL4/28 reaches up to 20 μm × 20 μm (Fig. 6(f)). Further, the occurrence of chlorite ($(Mg,Fe)_3(Si,Al)_4O_{10}(OH)_2 \cdot (Mg,Fe)_3(OH)_6$) and pyrite ($FeS_2$) in the forms of framboids (Fig. 3(b)) is observed within a large group of the investigated sediments. Chlorite is abundant in lithomembers C and A, whereas pyrite is prevalent in lithomembers A, B, and D (Table 4, Figs. 3, 4 and 6). Moreover, analcime is an essential constituent of the main mineral phase across all lithomembers, particularly within A, D, and C (Table 4). On the contrary, amphibole and pyroxene are exclusively detected in the lithomember C (BL4/8 and BL4/15).

The clay phase is dominant across the vast majority of the analyzed samples, with the exceptions of BL4/9 and BL4/14 of lithomember C, including BL4/28 of lithomember A. In the latter sequence, quartz and/or dolomite are prevalent (Table 4). Chlorite and muscovite are the main constituents of the clay phase, whereas smectite occurs among a large group of the investigated samples. The exceptions are BL4/10 (lithomember D), BL4/16 (lithomember A), and BL4/22 (lithomember B).

The observed diversity in accessory mineral phase ranges from samples with ferrous phases (hematite—Fe_2O_3, Fe-hydroxides) in lithomembers C and A, including those with widespread titanic/titanium-ferric phases (rutile—TiO_2, ilmenite—$FeTiO_3$, Ti-magnetite). There are also mineral phases that are observed in ultrabasic rocks, namely Cr-spinel—$(Mg,Fe^{2+})(Al,Cr,Fe^{3+})_2O_4$, pentlandite—$(Fe,Ni)_9S_8$, sepiolite—$Mg_4Si_6O_{15}(OH)_2 \cdot 6H_2O$ in lithomembers C, D, and A (Table 4). The presence of sphene ($CaTiSiO_5$) in sample BL4/17 (lithomember A), zircon ($ZrSiO_4$) in samples BL4/9 (lithomember C), BL4/10 (lithomember D), BL4/17 and BL4/28 (lithomember A) was found. Additionally, the occurrence of phosphates (apatite-$Ca_5(PO_4)_3(OH,F,Cl)$) in samples BL4/9 and BL4/14 (lithomember C), as well as in sample BL4/29 (lithomember A), whereas calcium sulfates (gypsum—$CaSO_4 \cdot 2H_2O$ or anhydrite—$CaSO_4$) was observed in samples BL4/7 (lithomember D) and BL4/8 (lithomember C) (Table 4).

4.3. Rock classification

The contents of calcite, dolomite, and fine-grained non-carbonate clastites suggest that the investigated sedimentary rocks are

Table 4
Mineral composition of samples from borehole BL4 based on SEM-EDS and X-ray analysis.

Minerals	Samples and lithomembers													
	D	C		D	C	C	A		B	A				
	BL4/7	BL4/8	BL4/9	BL4/10	BL4/14	BL4/15	BL4/16	BL4/17	BL4/21	BL4/22	BL4/27	BL4/28	BL4/29	BL4/30
Main mineral phase														
Quartz	+	+	++++	+	+++	++	+	+	+	+	++	+	+	++
Calcite	+	+	++		++	+			+		+			+
Dolomite	+	+	+	+		+		+	+	+	+	+++	++	
K-feldspar	+	+	++	+	++	+		+	+	+	+	+	+	+
Plagioclase	+	+	+	+	++	+		+	+	+	+	+		+
Chlorite			++	+	+		+	+		+		+	++	
Biotite					+			+		+		+		
Pyrite			+	++	+		+			+		++	+	
Analcime	++	++	+		+	+		+	++		+	+		
Amphibole		+												
Pyroxene						+								
Muscovite					+		+	+					+	
Clay minerals (illite/sericite, chlorite and smectite)	+++	+++	+	++++	+	+++	+++++	++++	+++	++++	+++	+	++	+++
Accessory mineral phase														
Ilmenite			*		*									
Hematite		*				*								
Sepiolite	*	*				*				*	*			
Gypsum/Anhydrite	*	*												
Ti-magnetite			*		*									
Apatite			*		*								*	
Zircon			*					*				*		
Fe-hydroxide			*	*	*		*							
Rutile				*	*			*		*		*	*	
Sphene								*						
Pentlandite			*											
Cr-spinel			*											

Plus signs (+) represent the abundance of each mineral. The abundance of specific minerals increases with the increasing number of plus signs; the asterisk sign (*) indicates that the mineral was found in the sample.

consistent with low-carbonate fine-grained clastites, in which a total carbonate content is less than 20% (Table 5, Fig. 7). Exclusively samples BL4/18 and BL4/28 of lithomember A include highly carbonated clastites, having contents above 20%, particularly sample BL4/28, which is dolomite-calcite marl with a carbonate content above 53% (Fig. 7).

4.4. Distribution of major elements

Table 6 and Fig. 8 demonstrate the change of the key major elements for the investigated lithomembers from borehole BL4. Significant variations in the content of sodium oxide (Na_2O), magnesium oxide (MgO), aluminum oxide (Al_2O_3), silicon dioxide (SiO_2), calcium oxide (CaO), titanium dioxide (TiO_2), and ferric oxide (Fe_2O_3) (Table 6, Fig. 8) are observed in all lithomembers. Nevertheless, the contents of potassium oxide (K_2O) and manganese oxide (MnO) seem to have a relatively constant value (average 0.13 and 2.83 wt%, respectively, Table 6).

Furthermore, the content of Na_2O and Al_2O_3, Na_2O and SiO_2, and Al_2O_3 and SiO_2, as well as of CaO and MgO, have a positive linear correlation for lithomembers A and B. The correlation coefficients (r) range from 0.86 to 0.95, respectively (Fig. S2 in the ESM). Therefore, their presence is consistent with quartz, analcime, dolomite, or clay phase (Table 6). For instance, the highest MgO and CaO content is registered for sample BL4/28 (lithomember A), which is rich in dolomite (Tables 4–6, Figs. 3, 4, and 6).

Interestingly, the correlation coefficients have either lower or negative values for lithomembers C and D (for Na_2O and Al_2O_3, Na_2O and SiO_2, and Al_2O_3 and SiO_2, r ranges from 0.025 to −0.23; whereas for CaO and MgO, $r = 0.42$, Fig. S2 in the ESM). Compared to lithomembers A and B, a more significant presence of amphibole, illite, muscovite, chlorite, or smectite in lithomembers C and D has

influenced the correlation coefficients. The interference with the correlation coefficients suggests that major elements have probably partitioned differently among the mineral components. On the other hand, the highest contents of K_2O, TiO_2, and Fe_2O_3 (3.52, 1.01, and 10.35 wt%, respectively, Table 6, Fig. 8) are registered in lithomember C at 118 m. Such a dependence is associated with a substantial presence of amphibole, illite, muscovite, chlorite, or smectite (Table 6, Figs. 3 and 4).

4.5. Organic-geochemical parameters

As listed in Table 7, the total organic carbon (Corg) contents vary between 0.32 and 1.40 wt% (Fig. 9(a)), whereas the amount of extractable organic matter (EOM) ranges from 158 to 2474 ppm. The highest concentration of EOM was measured in lithomember B at 413 m (2474 ppm, Table 7), corresponding to the highest amount of Corg.

The carbon/nitrogen (C/N) ratio values are generally under 10 for lithomembers A and B, whereas the values for lithomembers C and D are mostly between 10 and 20 (Table 7, Fig. 9(b)). On the other hand, the carbon/sulfur (C/S) ratio for a large group of investigated samples is under 10 (Table 7, Fig. 9(c)).

A dominance of long-chain (n-C_{27}, n-C_{29}, and n-C_{31}) over short-chain (n-C_{17}, n-C_{19}, and n-C_{21}) length n-alkanes is observed within sediments of borehole BL4 (n-C_{17}−n-C_{21}/n-C_{27}−n-C_{31} under 1, Table 7, Fig. 9(d)). However, somewhat higher portions of short-chain length n-alkanes are observed at 496, 541, 561, and 578 m (lithomember A (n-C_{17}−n-C_{21}/n-C_{27}−n-C_{31} over 0.44, Table 7, Fig. 9(d)). Both n-C_{27}/n-C_{31} and alkane index ($AI = n$-C_{31}/(n-$C_{31} + n$-C_{29})) indicate a predominance of n-C_{31} over n-C_{27} and n-C_{29} (Table 7). The terrigenous to aquatic (TAR) ratio reaches a value that is over 1 (Table 7) across the entire sample set, whereas the average
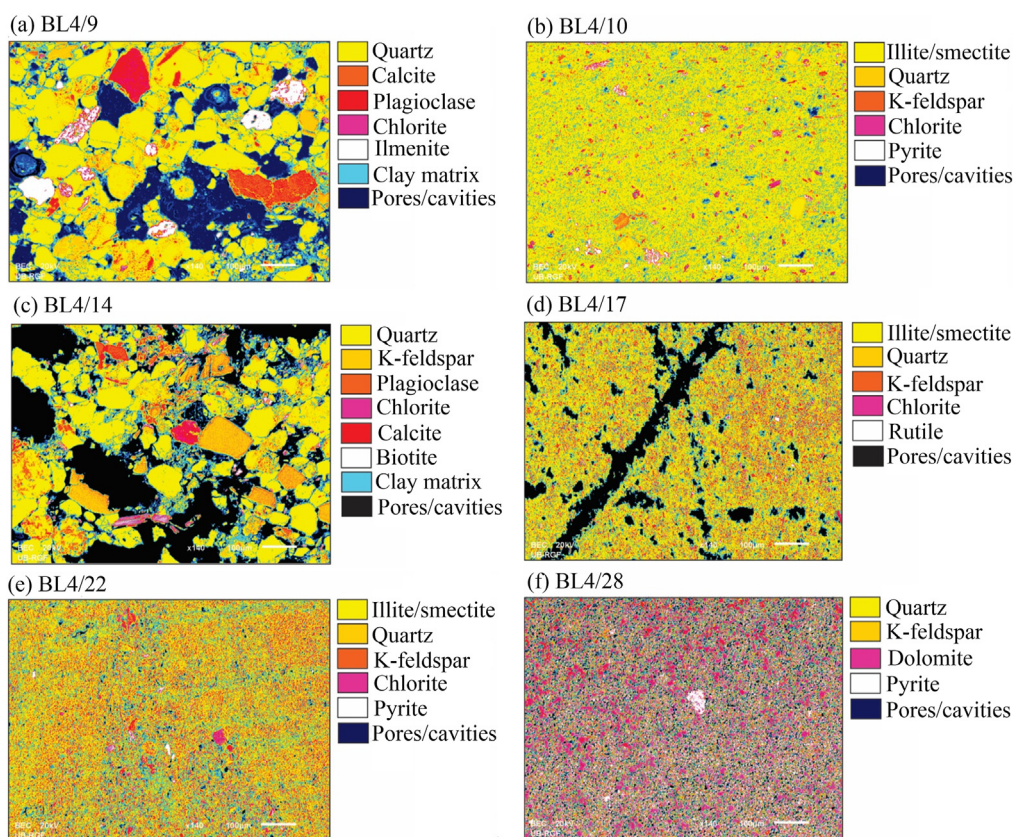
Fig. 6. Colored (BEC) images of representative samples from borehole BL4 ((a) and (c)) coarse-grained samples with dominant quartz, BL4/9 and BL4/14 (lithomember C); ((b), (d), and (e)) samples with dominant clay phase composition of illite/muscovite, chlorite, and smectite, BL4/10 (lithomember D), BL4/17 (lithomember A), and BL4/22 (lithomember B); (f) sample with dominant dolomite, BL4/28 (lithomember A).

Table 5
Complexometric determination of the percentage of CaO, MgO, calcite, and dolomite contents in the investigated samples from borehole BL4.

Sample	CaO	MgO	Calcite	Dolomite	ΣCalcite and dolomite
BL4/2	4.06	2.08	7.26	4.35	11.60
BL4/4	3.45	2.22	6.15	4.64	10.79
BL4/5	3.90	2.54	6.96	5.32	12.28
BL4/6	3.68	1.32	6.57	2.77	9.33
BL4/7	3.61	2.34	6.45	4.89	11.33
BL4/8	1.84	2.57	3.28	5.38	8.66
BL4/9	4.48	2.78	8.00	5.82	13.82
BL4/10	5.46	3.22	9.76	6.74	16.49
BL4/11	4.48	4.04	8.01	8.46	16.47
BL4/12	4.48	3.74	7.99	7.83	15.82
BL4/13	2.68	1.73	4.78	3.62	8.40
BL4/14	2.83	1.78	5.04	3.72	8.76
BL4/15	3.11	1.92	5.56	4.01	9.58
BL4/16	3.42	1.88	6.11	3.93	10.04
BL4/17	2.45	2.55	4.38	5.33	9.71
BL4/18	7.62	4.64	13.61	9.71	23.32
BL4/19	3.18	2.48	5.68	5.19	10.88
BL4/20	4.61	4.03	8.23	8.43	16.67
BL4/21	2.57	1.78	4.59	3.73	8.32
BL4/22	3.38	3.14	6.04	6.56	12.61
BL4/23	2.69	2.58	4.81	5.40	10.20
BL4/24	2.65	2.66	4.73	5.57	10.30
BL4/25	2.30	2.45	4.11	5.13	9.24
BL4/26	3.83	2.05	6.84	4.28	11.12
BL4/27	2.91	2.88	5.20	6.02	11.21
BL4/28	18.72	9.54	33.42	19.95	53.38
BL4/29	3.23	2.65	5.76	5.55	11.31
BL4/30	5.08	0.66	9.08	1.39	10.47
BL4/31	2.33	2.19	4.16	4.58	8.75

chain length parameter (ACL $= (25 \times n\text{-}C_{25} + 27 \times n\text{-}C_{27} + 29 \times n\text{-}C_{29} + 31 \times n\text{-}C_{31} + 33 \times n\text{-}C_{33})/(n\text{-}C_{25} + n\text{-}C_{27} + n\text{-}C_{29} + n\text{-}C_{31} + n\text{-}C_{33})$, Table 7) is averaging at 28.88.

Phytane (Ph) dominates over pristane (Pr) in all lithomembers (Pr/Ph under 1, Table 7). Additionally, higher concentrations of isoprenoids $i\text{-}C_{25}$ and $i\text{-}C_{30}$ are detected in lithomembers A and B ($i\text{-}C_{25}/n\text{-}C_{22}$ and $i\text{-}C_{30}/n\text{-}C_{26}$ ratios up to 0.16 and 0.71, respectively, Table 7, Fig. 9(e)). At the same time, the presence of β-carotane is observed in lithomembers A and B.

The S/H (steroid to hopanoid) ratio has values over 1, except for samples BL4/8 and BL4/15 (lithomember C, Table 7, Fig. 9(f)). The C_{31} homohopane ratio is mostly under 0.40 (Fig. 9(g)), whereas the C_{29} sterane ratio is below 0.09 in both units (Table 7). The gammacerane index (GI) values for all samples are over 1, reaching a maximum at 160 m of lithomember D (6.36, Table 7).

5. Interpretation

5.1. Geological, sedimentological, and mineralogical insights

The Toplica Basin can be characterized as a relic of a medium to large Neogene intermontagne-type paleolake, formed on top of the thinned Serbo-Macedonian basement unit, which had a role of Tethyan European margin (Marović et al., 2001; Schmid et al., 2008, 2020; Spahić & Gaudenyi, 2020). The paleolake's depth underwent extension, exposing the variations driven by a Neogene subsidence followed by the episodes of basin inversion. The Toplica basin ranges from being relatively shallow to having depocenters a few kilometers deep, largely depending on the Neogene
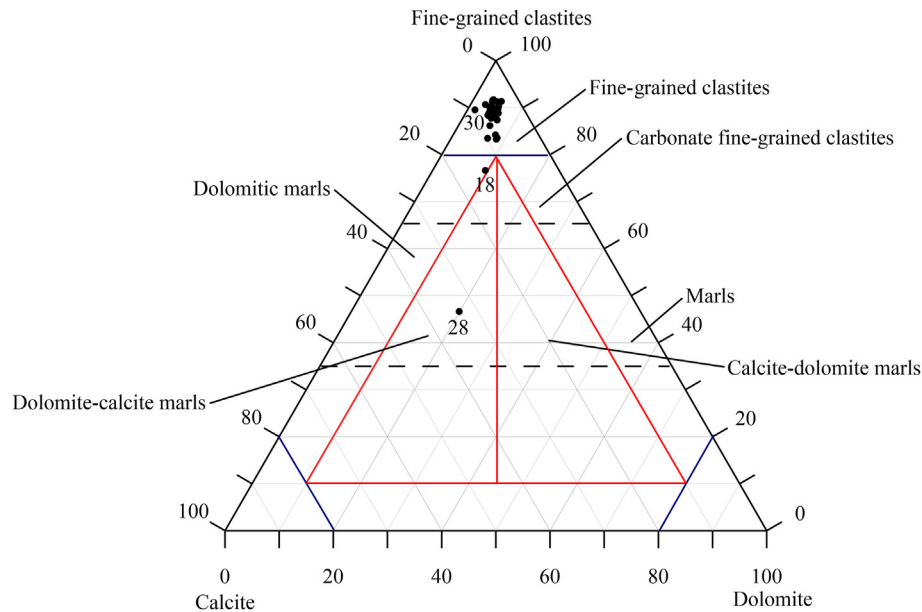
Fig. 7. Diagram of rock classification in the calcite—dolomite—fine-grained clastite system (according to Konta, 1969).

Table 6
The results of the XRF measurements for samples from borehole BL4.

Sample	Na$_2$O	MgO	Al$_2$O$_3$	SiO$_2$	K$_2$O	CaO	TiO$_2$	MnO	Fe$_2$O$_3$
BL4/7	5.00	5.10	18.40	42.31	2.69	4.93	0.61	0.12	6.85
BL4/8	2.56	5.25	19.46	39.44	3.52	1.29	1.01	0.05	10.35
BL4/10	3.64	5.10	18.23	42.31	2.93	4.08	0.70	0.12	6.59
BL4/11	3.62	5.81	15.92	37.77	2.79	5.57	0.59	0.14	6.87
BL4/15	2.04	3.49	17.14	45.61	3.08	2.74	0.73	0.12	7.45
BL4/19	4.26	3.77	17.76	42.42	2.79	3.56	0.66	0.13	7.35
BL4/21	3.87	3.69	17.40	41.27	3.00	3.77	0.68	0.13	6.05
BL4/22	3.22	3.98	16.77	40.57	3.06	2.68	0.62	0.13	7.04
BL4/23	3.84	4.13	16.52	38.95	2.76	4.12	0.64	0.14	6.02
BL4/25	4.02	3.93	17.57	41.47	3.02	2.53	0.67	0.13	7.08
BL4/26	2.28	3.10	14.67	35.07	2.74	3.95	0.68	0.15	7.69
BL4/27	2.29	2.83	15.54	35.40	2.83	1.69	0.67	0.12	8.05
BL4/28	0.93	7.50	8.74	19.64	1.43	16.45	0.30	0.17	6.32
BL4/29	2.09	3.43	15.77	37.78	2.88	2.92	0.65	0.13	7.75
BL4/30	2.56	2.91	15.56	37.18	2.96	2.66	0.64	0.15	8.13
Minimum	0.93	2.83	8.74	19.64	1.43	1.29	0.30	0.05	6.02
Maximum	5.00	7.50	19.46	45.61	3.52	16.45	1.01	0.17	10.35
Average	3.08	4.27	16.36	38.48	2.83	4.20	0.66	0.13	7.31

paleogeographic conditions controlling the levels of subsided basement. It appears the crustal-driven extension-related subsidence controlled the differentiation of Toplica basin depocenters (Figs. 1 and 10). The Toplica paleolake was mainly open, accommodating several inflowing supply channels, transporting eroded material from distinct near-marginal sources. The presence of analcime is consistent with the Neogene depositional cycles, indicating a constant supply of volcaniclastic material into the subsiding Toplica Basin. Analcime is formed by the transformation of transported volcanic material (Do Campo et al., 2007), mainly volcanic glass, which is likely connected with a Tertiary Lece Magmatic Complex. The adjoining Veliki Jastrebac granodiorite seems to be active and much older (47.59 ± 0.21 Ma emplacement age of the Ravnište pluton reflects exhumation and protracted cooling; Erak et al., 2017). Igneous activity in the close Lece Magmatic Complex began in the lower Oligocene and lasted during the middle Miocene (Burazer et al., 2021; Dragić et al., 2014; Malešević et al., 1974). Most sediments in the investigated chronostratigraphic section are consistent with alluvial-lacustrine and lacustrine facies (Fig. 2). The main structural feature of sediments is a horizontal lamination consistent with a calm, lacustrine sedimentary environment with very low energy (Reading, 2009).

The investigated lithologies of the lacustrine-type facies are fine-grained calcites and marls, with rare intercalations of sand (Fig. 2). The portion of the carbonate component is significant. The investigated lithomembers can be qualified as carbonate fine-grained clastites and marls (Fig. 2). The main lithotype is siltstone, having variations in argillaceous, terrigenous, and carbonate components. A prominent presence of authigenic iron sulfides, raspberry-shaped forms also referred to as framboids, is documented in a lower/older lacustrine sequence (below 285 m of depth, lithomembers A and B, Fig. 3(b)). Additionally, the upper section of the lacustrine series contains fossil fauna representatives, likely scattered redeposited fragments and remains of ostracods (Figs. 2 and 3(a)). Fossil remains become rare or absent with increasing depth, whereas in the alluvial-lacustrine sequence, exclusively some redeposited fragments are encountered (Figs. 2 and 3(f)).The occurrence of pyrite as framboids can serve as a paleoenvironmental indicator of paleoredox conditions (see Section 5.2.3; Wilkin & Barnes, 1996; Zatoń et al., 2008). On the other hand, the sporadic occurrence of sandstone layers in the upper part of the lacustrine unit (above 285 m of depth, lithomembers C and D, Fig. 2) is consistent with the periods of intensive terrigenous influx and sediment supply via alluvial flows (different near-marginal eroded rock sources).

The dominant rock types in this sequence are fine-grained siltstones with interlayers of fine-grained sandstones. Sandstones, often silty, mostly comprise quartz mixed with K-feldspar, chlorite, and calcite (Table 4, Figs. 3, 4 and 6). Further, the heavy mineral phase, mainly represented by ilmenite, hematite, sepiolite, gypsum/anhydrite, Ti-magnetite, apatite, zircon, Fe-hydroxide, and rutile, mainly characterizes the upper part of the lacustrine unit (Table 4). In contrast, the occurrence of Cr-spinel and pentlandite is noted only in lithomember C (BL4/9, Table 4). It seems that a higher portion of heavy minerals in the upper section of the lacustrine facies may suggest a mixed mafic and ultramafic source of eroded older rock fragments transported via alluvial flows (e.g., Dana, 2008; Gheith et al., 2021; Pujos et al., 1990; Salama et al.,
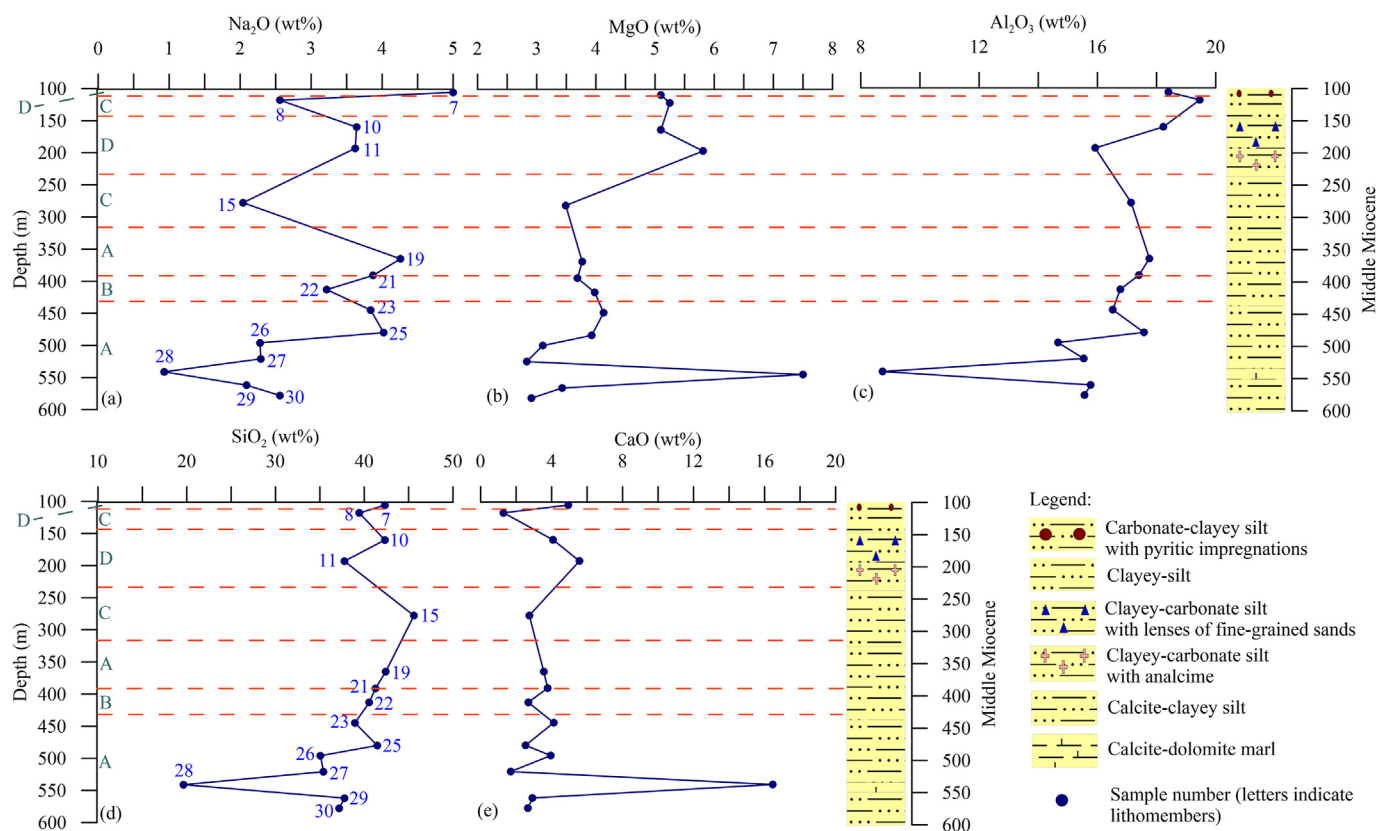
Fig. 8. The change of (a) Na₂O, (b) MgO, (c) Al₂O₃, (d) SiO₂, and (e) CaO with depth and simplistic lithostratigraphic representation for investigated sediments from borehole BL4.

2016). On the other hand, the presence of Cr-spinel may relate to Jurassic serpentinites (Aswad et al., 2011; Dana, 2008; Lužar-Oberiter et al., 2009; Fig. 1(c)), meaning that metamorphic rock fragments partially originate from the western and northwestern margins.

The terminal part of the drilled lithostratigraphic column is consistent with alluvial-lacustrine facies, characterized by fine-, medium-, and coarse-grained clastites. The base of the sequence comprises a package of sandstones, exhibiting a decreasing grain size trend directed upwards (Table 2) and fine-grained siltstones. Based on the main petrogenic components, sands belong to lithic arenites (Table 3). Higher contents of rock fragments and a noticeable difference in the stratigraphically interchanging content of heavy minerals (Table 3) are consistent with subaerial surface rock decomposition. Lastly, the occurrence of medium- and coarse-grained clastites suggests a slower closure of the Toplica paleolake.

5.2. Type of the OM, maturity, and paleoenvironmental implications

5.2.1. Type of the OM

The C/N ratio is consistent with a higher presence of nonvascular plants in lithomembers A and B (C/N under 10), while mixed portions of vascular and nonvascular plants are present in lithomembers C and D (C/N between 10 and 20, Meyers & Ishiwatari, 1993; Table 7, Fig. 9(b)). A more significant contribution of vascular plants in the OM appears in sample BL4/11 (Table 7, Fig. 9(b)). *n*-C₁₇−*n*-C₂₁/*n*-C₂₇−*n*-C₃₁ (under 1) and TAR (over 1) suggest vascular plants as dominant components of the OM in all lithomembers (Bush & McInerney, 2013; Cranwell et al., 1987; Eglinton & Hamilton, 1967; Ficken et al., 2000; Table 7). It should be considered that somewhat higher portions of short-chain length *n*-alkanes reflect the difference in sediments of

lithomember A (*n*-C₁₇−*n*-C₂₁/*n*-C₂₇−*n*-C₃₁ over 0.44, Table 7, Fig. 9(d)), further pointing to a higher presence of algae. Furthermore, grass vegetation and/or higher plants appear to be a substantial contributor to the OM because a general prevalence of *n*-C₃₁ over *n*-C₂₇ and *n*-C₂₉ is observed (*n*-C₂₇/*n*-C₃₁ under 1, AI over 0.50, and ACL from 28.03 to 29.78, Ficken et al., 2000; Table 7). The S/H ratio seems to correlate with the results of the C/N ratio, demonstrating an evident change between lithomembers A/B and C/D, from algal (over 1, Jiamo et al., 1990) to mixed algal/terrigenous and/or microbiologically reworked OM (Table 7, Fig. 9(f)). These results are consistent with a gradual transition between distinct paleoenvironments (see Section 5.2.3). On the other hand, the ambiguity of the parameters previously mentioned, particularly in the upper lacustrine segment, lies in the presence of resuspended OM. Such an OM results from the influx of older eroded rock fragments transported by alluvial flows (see Section 5.1), implicating that OM reflects both younger and older depositional cycles.

5.2.2. Maturity of the OM

In general, highly abundant Δ²,⁴,⁵ sterenes in sample BL4/8 (lithomember C), low C₃₁ homohopane, and C₂₉ sterane ratios point out that the OM deposited in all lithomembers is rather in the immature stage (Larcher et al., 1987; Peters & Moldowan, 1991; Seifert & Moldowan, 1980; Table 7, Fig. 9(g)). Nevertheless, the C₃₁ homohopane ratio has displayed a few variations in the OM maturity at intervals of 118 and 278 m of lithomember C (0.54 and 0.46, respectively, Table 7, Fig. 9(g)). A higher thermal evolution of the OM in these sediments may relate to a paleo-heat flow provoked by a constant influx of volcanoclastic material, evidenced by the presence of analcime in lithomember C (Tables 4 and 7, Fig. 9(g)).

Table 7
The results of group and specific organic geochemical parameters for selected samples of borehole BL4, calculated from the distribution and relative abundance of *n*-alkanes, isoprenoids, steroids, and terpenoids.

Sample	Corg[a]	EOM[b]	C/N[c]	C/S[d]	$n\text{-}C_{17}\text{-}n\text{-}C_{21}/n\text{-}C_{27}\text{-}n\text{-}C_{31}$	$n\text{-}C_{27}/n\text{-}C_{31}$	AI[e]	TAR[f]	ACL[g]	Pr/Ph[h]	$i\text{-}C_{25}/n\text{-}C_{22}$[i]	$i\text{-}C_{30}/n\text{-}C_{26}$[j]	Relative abundance of β-carotane (*m/z* 125)	S/H[k]	$C_{29}S/(R+S)$[l]	$C_{31}S/(S+R)$[m]	GI[n]
7	0.79	1074	14.21	3.97	0.19	0.74	0.50	18.86	28.89	0.03	0.10	0.31	−[o]	1.77	0.04	0.21	4.56
8	0.34	322	12.60	0.58	0.27	1.01	0.51	7.42	28.79	0.28	0.11	0.24	−	0.52	ND[r]	0.54	2.08
10	0.64	1791	11.78	1.33	0.25	0.62	0.55	14.68	29.15	0.06	0.11	0.15	−	1.81	0.05	0.29	6.36
11	0.43	880	18.43	6.20	0.22	0.57	0.57	8.62	29.43	0.27	ND	ND	−	1.36	0.03	0.22	5.78
15	0.32	158	3.34	ND	0.37	0.90	0.50	7.93	28.25	0.10	0.09	0.18	−	0.48	0.08	0.46	4.83
19	0.44	439	6.46	2.18	0.32	0.67	0.59	9.94	29.08	0.03	0.10	0.66	+[p]	7.60	0.03	0.33	1.81
21	0.50	435	6.14	17.56	0.31	0.86	0.50	13.06	28.79	0.04	0.07	0.71	++[q]	6.37	0.05	0.22	1.49
22	1.40	2474	12.72	8.55	0.19	0.41	0.57	8.63	29.63	0.05	0.14	0.24	++	7.20	0.07	0.04	1.03
23	0.76	791	10.75	ND	0.33	0.59	0.57	12.57	29.17	0.06	0.03	0.30	++	7.51	0.06	0.22	1.31
25	0.78	614	10.86	14.67	0.17	0.44	0.60	16.26	29.78	0.09	0.07	0.45	++	7.02	0.09	0.28	1.29
26	0.58	480	6.78	2.73	0.60	0.98	0.57	6.11	28.51	0.05	0.11	0.16	++	4.51	0.06	0.36	2.80
27	0.65	366	9.24	1.88	0.30	0.94	0.56	7.38	28.63	0.09	0.06	ND	+	4.76	0.05	0.27	5.42
28	0.41	178	8.63	2.90	0.61	1.34	0.50	7.64	28.03	0.03	0.16	0.18	+	3.05	0.06	0.25	5.86
29	0.48	396	5.91	1.36	0.44	0.76	0.54	6.49	28.64	0.04	0.11	0.17	+	3.47	0.06	0.24	4.73
30	0.39	259	5.47	7.39	0.49	0.93	0.54	7.70	28.43	0.05	0.06	0.26	+	2.27	0.08	0.32	3.06
Minimum	0.32	158	3.34	0.58	0.17	0.41	0.50	6.11	28.03	0.03	0.03	0.15	/	0.48	0.03	0.04	1.03
Maximum	1.40	2474	18.43	17.56	0.61	1.34	0.60	18.86	29.78	0.28	0.16	0.71	/	7.60	0.09	0.54	6.36
Average	0.59	710	9.56	5.48	0.34	0.79	0.54	10.22	28.88	0.08	0.09	0.31	/	3.98	0.06	0.28	3.49

[a] Corg—the content of organic carbon (wt.%).
[b] EOM—extractable organic matter (ppm).
[c] Molar ratio of C/N.
[d] Molar ratio of C/S.
[e] AI—alkane index = $n\text{-}C_{31}/(n\text{-}C_{31} + n\text{-}C_{29})$.
[f] TAR—terrigenous/aquatic ratio = $(n\text{-}C_{27} + n\text{-}C_{29} + n\text{-}C_{31})/(n\text{-}C_{15} + n\text{-}C_{17} + n\text{-}C_{19})$.
[g] ACL—average chain length = $(25 \times n\text{-}C_{25} + 27 \times n\text{-}C_{27} + 29 \times n\text{-}C_{29} + 31 \times n\text{-}C_{31} + 33 \times n\text{-}C_{33})/(n\text{-}C_{25} + n\text{-}C_{27} + n\text{-}C_{29} + n\text{-}C_{31} + n\text{-}C_{33})$.
[h] Pr/Ph = pristane/phytane.
[i] i_{25}—C_{25} regular isoprenoid.
[j] Sq—C_{30} irregular isoprenoid (squalane).
[k] S/H—$\sum$Steroids/$\sum$Hopanoids = $\sum C_{27-29}$ ααα(S + R)-steranes or $\sum C_{27-29}$ ($\Delta^2 + \Delta^4 + \Delta^5$)-sterenes/$\sum C_{29-33}$ αβH-hopanes.
[l] C_{29} (20S)/(20S + 20R) = C_{29} sterane ααα20(S)/C_{29} sterane ααα20(S) + C_{29} sterane ααα20(R).
[m] C_{31} (22S)/(22S + 22R) = C_{31}homohopane (22S)/(22S + 22R).
[n] GI (Gammacerane index) = $10 \times$ Gammacerane/(Gammacerane + C_{30}-hopane).
[o] − β-carotane was not detected.
[p] + low abundance of β-carotane
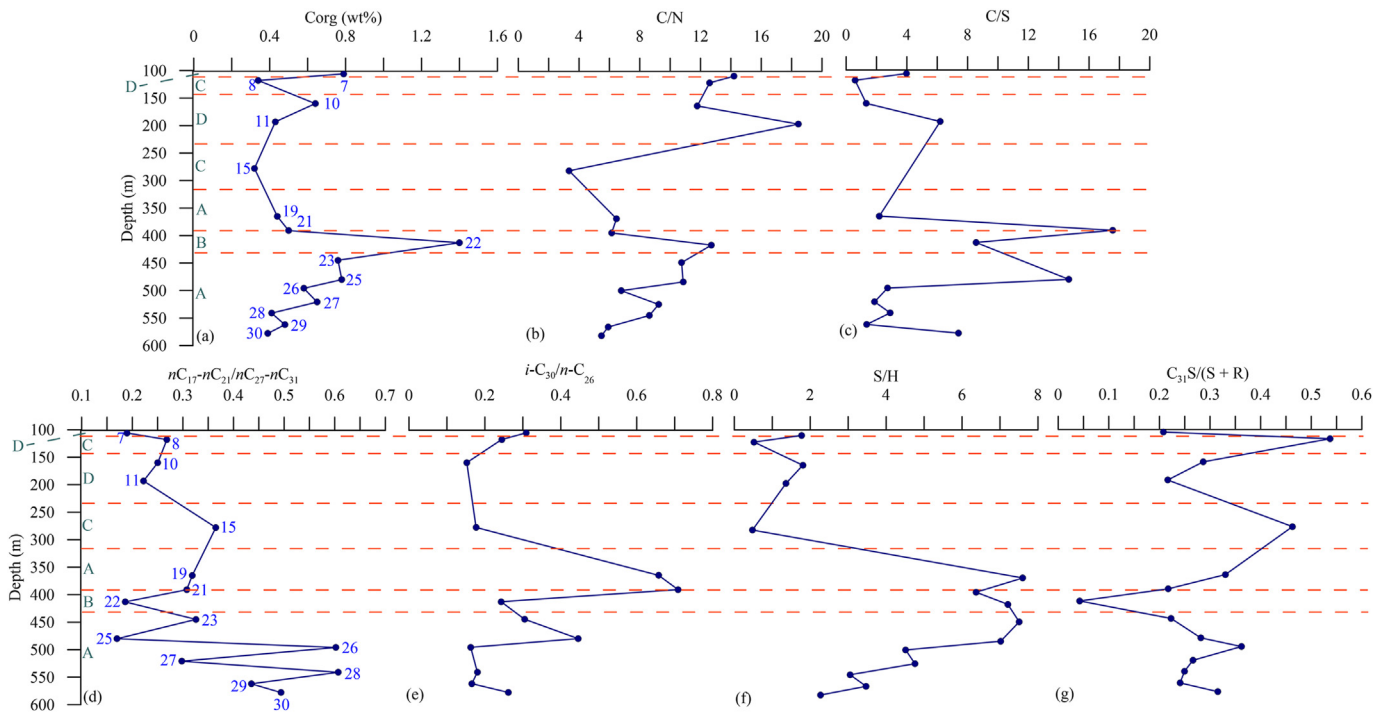[q] ++ high abundance of β-carotane.
[r] ND—Not Determined.

Fig. 9. The change of (a) C_{org}, (b) C/N, (c) C/S, (d) n-C_{17}−n-C_{21}/n-C_{27}−n-C_{31}, (e) i-C_{30}/n-C_{26}, (f) S/H, and (g) $C_{31}S/(S + R)$ with depth for investigated sediments from borehole BL4.

5.2.3. Paleoenvironmental conditions

Oxygen depletion (Pr/Ph under 0.10), alkaline (i-C_{25}/n-C_{22} up to 0.16), and saline (C/S mostly under 10, i-C_{30}/n-C_{26} up to 0.71, and GI over 1) conditions are mainly responsible for preservation and accumulation (Corg up to 1.40 wt%) of the OM within lithomembers A and B (Berner & Raiswell, 1984; Didyk et al., 1978; Grice et al., 1998; Leventhal, 1987; Sinninghe Damasté et al., 1995; Table 7, Fig. 9(c) and 9(e)). Additionally, the presence of pyrite framboids reveals that sediment deposition has occurred in the anoxic portion of the water column (Wilkin & Barnes, 1996; Zatoń et al., 2008; Fig. 3(b)). Furthermore, the occurrence of β-carotane in lithomembers A and B unambiguously corroborates that the deposition occurred under calm saline and anoxic lacustrine conditions (Grba et al., 2014; Jiang & Fowler, 1986; Table 7). At the same time, the depositional conditions in lithomembers C and D seem slightly different once compared to lithomembers A and B. The absence of β-carotane, a lower concentration of i-C_{25} and i-C_{30}, and a fluctuating Pr/Ph ratio (Pr/Ph up to 0.28) may suggest anoxic−dysoxic freshwater lacustrine conditions, consistent with lower contents of Corg (Table 7). However, higher sedimentation rates are likely responsible for its preservation in these lithomembers, corresponding to recently emphasized higher subsidence rates (Spahić et al., 2023). On the other hand, the dynamics of alluvial-lacustrine processes, which transported sequences of sand and gravel (samples in the lithomembers C and D), are likely responsible for diluting and reducing the OM contents in these sediments. A straightforward example is sample BL4/9, which is rich in heavy minerals (Table 4), resulting from the erosion processes of nearby lithomembers with a lower content of the OM (Corg under 0.1 wt%).

6. Discussion

6.1. A local-scale geological, sedimentological, and geochemical interpretation of the depositional process in borehole BL4

Recent investigations of the Toplica Basin have underscored a mineralogical and OM composition of sediments from central

(borehole BL3 and BL5—eastern segment) as well as northwestern (borehole BL7—western segment) depocenters. Based on the tectonic activity of the studied area and the borehole location, the studied segment represents some form of the inner basinal "barrier" connecting and disconnecting the eastern and western depocenters of the Toplica Basin. It appears that Neogene subsidence of the Toplica graben system, with its interdependent tectonic-sedimentological processes, was strongly influenced by its immediate surrounding (e.g., elevation or tectonic exhumation of the Jastrebac core-complex; Marović et al., 2007c; Erak et al., 2017). The influence on the paleolake by the abutting landmasses is well-documented by the mineralogical and geochemical variations.

According to the mineralogical composition, lithomembers A and B are characterized by a dominant presence of analcime (from altered volcanic material), clay, and carbonate minerals, particularly dolomite, followed by pyrite concretions (Table 4, Figs. 2, 4 and 6). Moreover, the predominance of phytane, higher concentrations of i-C_{25} and i-C_{30}, followed by the occurrence of β-carotane, together with the mineral composition (Tables 4−7) indicate that the depositional environment was rather calm, saline, anoxic, and stacked with volcanic ash nutrients. The presence of pyrite framboids further corroborates previous observations. Such an environment prompts a proliferation of bacterial and algal communities, enhancing the primary productivity (Corg up to 1.40, S/H over 1, Table 7). The results show similarities in the mineral compositions and organic geochemical characteristics connecting the Prebreza and the Čučale sediments of borehole BL7 with lithomembers A and B.

During the initial extensional core-complex-related basin development stage and deposition of lacustrine facies (formation of the deeper lithomembers A and B; Fig. 10(a)#1−2), the investigated graben system somehow hindered the material transportation observed in the eastern basin sequences (boreholes BL3 and BL5). The exhumation of the Jastrebac dome could be the mechanism lifting the structural basin high at the paleo-lake bottom. This process, in particular, is consistent with the associated mylonite structures and detachment plane reported from the central part of
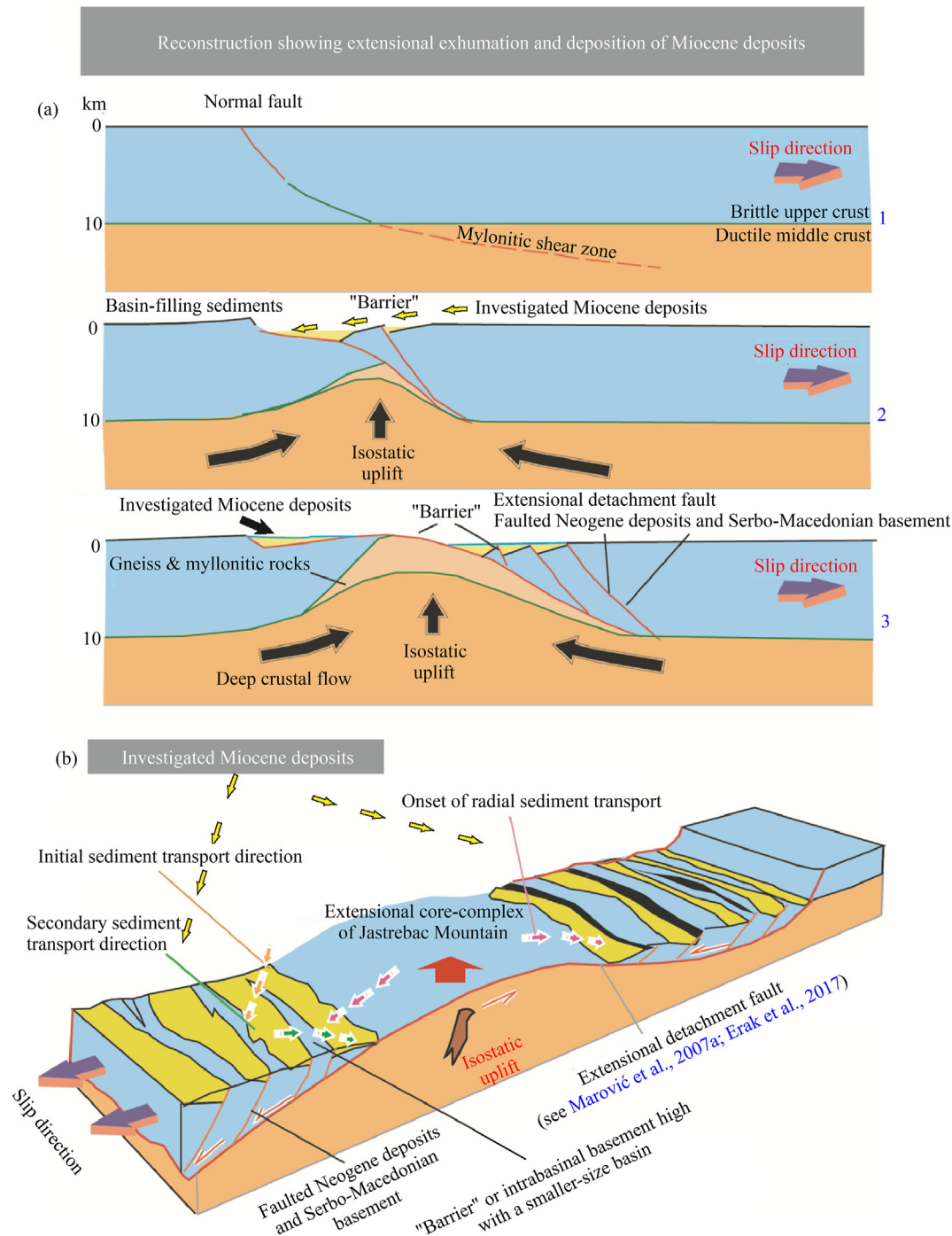
Fig. 10. Schematic diagram of the possible mechanism yielding the Jastrebac core complex and the role of "barrier" in the Toplica Basin (inset for Fig. 10(a) taken from Spencer, 2006, modified). (a) Idealized cross-sectional evolution of extensional exhumation of a metamorphic core complex, applied to the Jastrebac Mountain (Mt.). Rapid extension affected the isostatic uplift in response to tectonic denudation (blue layer), extruding from the plastically deforming middle crust to the Earth's surface. (1) Extensional offset and formation of the main detachment fault within the Serbo-Macedonian Unit. (2) Formation of tilted early graben system with widely exposed mylonitic and gneissic rocks derived from the middle crust (Erak et al., 2017; Marović, Đoković, Toljić, Milivojević et al., 2007a). The ongoing extension and progressing exhumation or isostatic uplift and crustal stretching produced accommodation space for the basin. The main direction of material inflow is from the abutting protruded areas (not from exposed footwall). (3) The progressive extensional uplift closed the main source, redirecting the material transport in the opposite direction. (b) Hypothetical three-dimensional (3D) block diagram exposing the progressing core complex and crust extension with deposition. The "barrier" was likely very near to a progressing dome intervening with the deeper segments of the Toplica Basin.

Jastrebac Mountain (Erak et al., 2017; Fig. 10(a)#1). Simultaneously with the regional extension, the subsidence of the Toplica graben system "opened" a sediment transport channel, allowing sourcing and sediment supply directed towards the western basin depocenter (Fig. 10(a)#2). In addition to reported detachment planes and mylonitic zones, such an interpretation emerged from

comparing the mineralogical and the organic geochemical features depicted in sediments from the available boreholes BL7 and BL4.

The opposite scenario of the sediment supply and transport behavior has likely occurred during the deposition of the upper lithomembers C and D (Fig. 10(a)#3). The change in the position or the uplift of the depocenter's intervening structural high likely

produced the opposite direction of sediment delivery (Fig. 10(b)). The presence of quartz, analcime, and clay minerals, as well aspyritic concretions, is noted in these sequences (Table 4, Figs. 2–4 and 6). A greater presence of quartz relates to thicker sandy clasts with OM particles transported via the alluvial-lacustrine system (Fig. 2). On the other hand, some fluctuations in the Pr/Ph ratio (values near 0.30), lower concentrations of i-C_{25} and i-C_{30}, and absence of β-carotane indicate anoxic–dysoxic freshwater lacustrine conditions, further affecting the content of OM in these lithomembers. A dilution factor should not be excluded since a higher contribution of clay minerals and sand may be responsible for the OM reduction. To underline, the tectonic interplay of the Toplica graben affected the formation of lithomembers C and D, this time by inverting the sediment transport direction (Fig. 10(b)). At this point, the sediment characteristics and paleoenvironmental settings correspond to material typical for the eastern basin sequences (boreholes BL3 and BL5). Such asymmetric deposition suggests that the graben system prevented sediment supply from the basin's western side (Fig. 10(a)#3). The terminal stage of developing the lacustrine depositional environment change is followed by the formation of alluvial-lacustrine facies, representing the final basin cycle. The alluvial-lacustrine system has transported larger-size clasts into the basin, indicating the terminal paleolake stage and slow closure of the Toplica Basin.

6.2. Regional-scale depositional patterns and comparison with neighboring basins

The basin location is in an intervening position between the extensional-type tectonic influence of the Pannonian back-arc stretching and the Aegean Oligo-Miocene extensional realms (Burchfiel et al., 2008, 2018; Fodor et al., 2021; Marović, Đoković, Toljić, Milivojević et al., 2007a; Matenco & Radivojević, 2012; Spahić, 2022a; Fig. 1(a)). The area of the Toplica Basin and its surroundings represents an extremely complex former (Paleo)Tethyan margin and its overriding plate (e.g., Erak et al., 2017; Marović et al., 2007a; Schmid et al., 2008; Spahić & Gaudenyi, 2019; Spahić and Gaudenyi, 2022; Spahić, 2022b; Fig. 1(a)). An additional peculiarity observed within the basin deposition itself lies in the evolution of the nearby Jastrebac Mountain dome and a Neogene metamorphic core complex (Fig. 1(c)). The Neogene deposition was coeval with the extensional-type crustal uplifting, the process which allowed exhumation of deep crustal rocks across the thinned Serbo-Macedonian crust (tectonics-related phenomenon well-recorded across the Balkans; Balázs et al., 2016; Erak et al., 2017; Fodor et al., 2021; Fügenschuh & Schmid, 2005; Marović et al., 2007b, 2007c; Menant et al., 2016; Tari et al., 2020). Thus, the Neogene Toplica Basin is almost entirely developed on top of the crystalline rocks belonging to the Lower Paleozoic Serbo-Macedonian Unit, whereby a smaller portion might be on top of the Supragetic greenschist-facies rocks (Erak et al., 2017; Marović et al., 2007a, 2007b; Fig. 1(c)).

In response to such localized, crustal-driven subsidence and deposition, the Central and South-Eastern European basins were filled mainly with abundant freshwater and brackish systems of the Neogene, which coexisted with Oligocene–middle Miocene Central Paratethys (e.g., Mandić et al., 2011; Mandić, et al., 2019a; Rundić et al., 2013; Rundić, 2022). These tectonic sub-basins provided accommodation space for a number of lake basins characterized by alluvial, swamp, and lacustrine facies, reaching a total of about 2000 m of depth (Obradović et al., 2007). Diverse lacustrine sediments were deposited, often alternating with alluvial and swamp sediments. The observed cyclicity of facies gave different facies accommodated during the basin evolution. Cyclicity is consistently observed across the Valjevo-Mionica,

Jadar, Aleksinac, Belanovica, and Pranjani basins (Andrić-Tomašević et al., 2021; Lazarević et al., 2019; Marić et al., 2019b; Obradović et al., 2007; Fig. 1). These depositional features slightly differ from the Neogene basin in the area of Inner Dinarides (Ugljevik, Lopare, Tuzla of Inner Dinarides; Bosnia & Herzegovina; de Leeuw et al., 2011; Grba et al., 2015; Mandić, et al., 2019a; Šajnović et al., 2008, 2020).

Although at a short distance, the region's basin opening conditions differ significantly and are difficult to compare, mainly because of the absence of deeper subsurface data (e.g., in the Toplica Basin, data are mainly based on the extracted cores from boreholes). Despite the synchronicity of their subsidence period, the basins cannot be connected in the regional context mainly because of significant differences in lithofacial development (Balázs et al., 2018; Cohen, 2003; Fornari et al., 2001; Harzhauser & Mandić, 2008; Lone et al., 2018; Meyers & Ishiwatari, 1993; Meyers & Lallier-Vergès, 1999; Mandić et al., 2019a, 2019b; Marić et al., 2019a, Obradović & Vasić, 2007; Scott et al., 2012). The composition of Neogene sediments is mainly regulated by paleo-relief and paleo-lake processes, depending on the lithological characteristics of the sediment catchment area involving paleoclimatic conditions. Each particular basin had different paleo-sourcing areas, further controlled by the subsidence rates. Important differentiation in the Miocene fault activity that largely subdivided different lithospheric-scale blocks with their subsiding properties resulted in a specific history of vertical mobility episodes (Marinović & Rundić, 2020; Marović et al., 2007c; Meulenkamp & Sissingh, 2003; Radivojević, 2023; Spahić et al., 2023).

7. Conclusions

The composite study of the middle Miocene sedimentary sequence elaborates on the superimposition of lacustrine sediments drilled across the northwestern or shallower Toplica Basin depocenter (borehole BL4, depth up to 630 m). The investigated segment of the Toplica Basin involved geological, sedimentological, mineralogical, inorganic, and organic geochemical analyses. The study additionally provides tectonic insights by analyzing thirty-one selected samples from the four Neogene sedimentary lithomembers, A, B, C, and D.

The lithospheric-scale extensional graben system of the Neogene age, developed across the underlying Serbo-Macedonian Unit, was the main factor controlling the investigated Neogene depositional processes and sediment delivery. The subsiding fault-controlled graben system and rising Jastrebac core-complex controlled both the material inflow delivered from exposed older rocks and the emerging lower Miocene sequence deposited during the syn-rift phase of the basin evolution. During the initial basin development stage (deposition of lithomembers A and B), the sediment sourcing "barrier" or intrabasinal high prevented a sediment supply towards the eastern Toplica depocenter. Such an intrabasinal configuration facilitated the material transport into the western depocenter (location of borehole BL7). Similar to borehole BL7, the depositional environment during the initial stage had a rather calm, saline, anoxic character that interfered with volcanic equivalents containing volcanic ash nutrients (presence of analcime and pyritic concretions; and framboidal forms). In addition, the current results show a predominance of phytane and higher concentrations of i-C_{25} and i-C_{30}, followed by the occurrence of β-carotane. Such a paleoenvironmental setting prompted a proliferation of bacterial and algal communities, which were substantiated by a considerably high S/H ratio.

After the sediment deposition of lithomember B finished, the graben system "opened" an opposite sediment-transportation path towards the eastern depocenter of the basin (position of boreholes

BL3 and BL5). In tectonic terms, this process is likely associated with the uplift and increasing elevation of the Jastrebac core complex. The extensional uplift during this stage of the middle Miocene behaved as a "barrier", prompting the deposition of capping C and D lithomembers. During this stage, the paleoenvironment was characterized as anoxic–dysoxic freshwater lacustrine having a higher contribution of terrestrial OM. A greater presence of terrestrial OM is consistent with a contemporary elevation and rise of the Jastrebac core complex. In this case, biomarkers demonstrate the fluctuations in the Pr/Ph ratio (values near 0.30), lower concentrations of i-C$_{25}$ and i-C$_{30}$, and the absence of β-carotene, with a somewhat higher S/H ratio. After the deposition of lithomember D, the successor alluvial-lacustrine environment represents the basin's terminal stage. The sediment supply and inflow of larger-size clasts mark the final depositional environment change and the gradual filling of the entire Toplica Basin.

Funding

Declaration of competing interest

The authors declare that they have no known competing financial interests or personal relationships that could have appeared to influence the work reported in this paper.

Acknowledgements

Appendix A. Supplementary data

Supplementary data to this article can be found online at https://doi.org/10.1016/j.ijsrc.2024.03.006.

References

Allen, P. A., & Allen, J. R. (2013). *Basin analysis: Principles and application to petroleum play assessment* (3rd ed.). Hoboken, NJ, U.S.: John Wiley & Sons, Ltd.

Andrić-Tomašević, N., Simić, V., Mandic, O., Životić, D., Suárez, M., & García-Romero, E. (2021). An arid phase in the internal Dinarides during the early to middle Miocene: Inferences from Mg-clays in the Pranjani Basin (Serbia). *Palaeogeography, Palaeoclimatology, Palaeoecology, 562*, 110145.

Antić, M., Peytcheva, I., von Quadt, A., Kounov, A., Trivić, B., Serafimovski, T., … Wetzel, A. (2016). Pre-Alpine evolution of a segment of the North-Gondwanan margin: Geochronological and geochemical evidence from the central Serbo-Macedonian Massif. *Gondwana Research, 36*, 523–544.

Aswad, K., Aziz, N., & Koyi, H. (2011). Cr-spinel compositions in serpentinites and their implications for the petrotectonic history of the Zagros Suture Zone, Kurdistan Region, Iraq. *Geological Magazine, 148*, 802–818.

Balázs, A., Magyar, I., Matenco, L., Sztanó, O., Tőkés, L., & Horváth, F. (2018). Morphology of a large paleo-lake: Analysis of compaction in the Miocene-Quaternary Pannonian Basin. *Global and Planetary Change, 171*, 134–147.

Balázs, A., Maţenco, L., Granjeon, D., Alms, K., François, T., & Sztanó, O. (2021). Towards stratigraphic-thermo-mechanical numerical modelling: Integrated analysis of asymmetric extensional basins. *Global and Planetary Change, 196*, 103386.

Balázs, A., Matenco, L., Magyar, I., Horváth, F., & Cloetingh, S. (2016). The link between tectonics and sedimentation in back-arc basins: New genetic constraints from the analysis of the Pannonian Basin. *Tectonics, 35*, 1526–1559.

Bartha, I. R., Botka, D., Csoma, V., Katona, L. T., Tóth, E., Magyar, I., … Sztanó, O. (2022). From marginal outcrops to basin interior: A new perspective on the sedimentary evolution of the eastern Pannonian Basin. *International Journal of Earth Sciences, 111*, 335–357.

Berner, R. A., & Raiswell, R. (1984). C/S method for distinguishing freshwater from marine sedimentary rocks. *Geology, 12*, 365–368.

Budai, S., Sebe, K., Nagy, G., Magyar, I., & Sztanó, O. (2019). Interplay of sediment supply and lake-level changes on the margin of an intrabasinal basement high in the Late Miocene Lake Pannon (Mecsek Mts., Hungary). *International Journal of Earth Sciences, 108*, 2001–2019.

Burazer, N., Šajnović, A., Kašanin-Grubin, M., Gajica, G., Orlić, J., Radisavljević, M., & Jovančićević, B. (2021). Early–Middle Miocene paleoenvironmental and paleoclimate changes in the Toplica Basin (Serbia) inferred from plant biomarkers, biochemical and elemental geochemical proxies. *Geologica Carpathica, 72*, 406–424.

Burazer, N., Šajnović, A., Vasić, N., Kašanin-Grubin, M., Životić, D., Mendonça Filho, J. G., … Jovančićević, B. (2020). Influence of paleoenvironmental conditions on distribution and relative abundance of saturated and aromatic hydrocarbons in sediments from the NW part of the Toplica basin, Serbia. *Marine and Petroleum Geology, 115*, 104252.

Burchfiel, B. C., Nakov, R., Dumurdzanov, N., Papanikolaou, D., Tzankov, T., Serafimovski, T., … Nurce, B. (2008). Evolution and dynamics of the Cenozoic tectonics of the South Balkan extensional system. *Geosphere, 4*, 919–938.

Burchfiel, B. C., Royden, L. H., Papanikolaou, D., & Pearce, F. D. (2018). Crustal development within a retreating subduction system: The Hellenides. *Geosphere, 14*, 1119–1130.

Bush, R. T., & McInerney, F. A. (2013). Leaf wax *n*-alkane distributions in and across modern plants: Implications for paleoecology and chemotaxonomy. *Geochimica et Cosmochimica Acta, 117*, 161–179.

Cohen, A. S. (2003). *Paleolimnology: The history and evolution of lake systems*. Oxford, U.K.: Oxford University Press.

Cranwell, P. A., Eglinton, G., & Robinson, N. (1987). Lipids of aquatic organisms as potential contributors to lacustrine sediments-II. *Organic Geochemistry, 11*, 513–527.

Dana, J. D. (2008). *Dana's new mineralogy-Revised edition*. Kingston, Jamaica: Merchant Books.

de Leeuw, A., Mandic, O., de Bruijn, H., Marković, Z., Reumer, J., Wessels, W., Šišić, E., & Krijgsman, W. (2011). Magnetostratigraphy and small mammals of the Late Oligocene Banovići basin in NE Bosnia and Herzegovina. *Palaeogeography, Palaeoclimatology, Palaeoecology, 310*, 400–412.

Didyk, B. M., Simoneit, B. R. T., Brassell, S. C., & Eglinton, G. (1978). Organic geochemical indicators of paleoenvironmental conditions of sedimentation. *Nature, 272*, 216–222.

Dimitrijević, M. D. (2000). The Dinarides and the Vardar Zone: The eternal conundrum. In S. Karamata & S. Janković (Eds.), *Proceedings of the International Symposium Geology and Metallogeny of the Dinarides and the Vardar Zone*. Banja Luka, Republic of Srpska: Academy of Sciences and Arts.

Divljan, S. (1979). Some petrological, mineralogical and geochronological characteristics of granitoid rocks of Mali Jastrebac Mts. (Central Serbia). *Radovi Geoinstituta, 13*, 141–160. *(In Serbian)*

Do Campo, M., del Papa, C., Jiménez-Millán, J., & Nieto, F. (2007). Clay mineral assemblages and analcime formation in a Palaeogene fluvial–lacustrine sequence (Maíz Gordo Formation Palaeogen) from northwestern Argentina. *Sedimentary Geology, 201*, 56–74.

Dragić, D., Mišković, A., Hart, C., Tosdal, R., Fox, P., & Glišić, S. (2014). Spatial and temporal relations between epithermal and porphyry style mineralization in the Lece Magmatic Complex, Serbia. In *Proceedings of the SEG Conference Building Exploration Capability for the 21st Century. September 27–30, 2014*. Keystone, CO, U.S.: Society of Economic Geologists.

Duggen, S., Croot, P., Schacht, U., & Hoffmann, L. (2007). Subduction zone volcanic ash can fertilize the surface ocean and stimulate phytoplankton growth: Evidence from biogeochemical experiments and satellite data. *Geophysical Research Letters, 34*, L01612.

Eglinton, G., & Hamilton, R. J. (1967). Leaf epicuticular waxes. *Science, 156*, 1322–1335.

Erak, D., Matenco, L., Toljić, M., Stojadinović, U., Andriessen, P. A. M., Willingshofer, E., & Ducea, M. N. (2017). From nappe stacking to extensional detachments at the contact between the Carpathians and Dinarides—The Jastrebac Mountains of Central Serbia. *Tectonophysics, 710–711*, 162–183.

Faccenna, C., Becker, T. W., Auer, L., Billi, A., Boschi, L., Brun, J. P., … Serpelloni, E. (2014). Mantle dynamics in the Mediterranean. *Reviews of Geophysics, 52*, 283–332.

Ficken, K. J., Li, B., Swain, D. L., & Eglinton, G. (2000). An *n*-alkane proxy for the sedimentary input of submerged/floating freshwater aquatic macrophytes. *Organic Geochemistry, 31*, 745–749.

Fodor, L., Balázs, A., Csillag, G., Dunkl, I., Héja, G., Jelen, B., … Vrabec, M. (2021). Crustal exhumation and depocenter migration from the Alpine orogenic margin towards the Pannonian extensional back-arc basin controlled by inheritance. *Global and Planetary Change, 201*, 103475.

Fornari, M., Risacher, F., & Féraud, G. (2001). Dating of paleolakes in the central Altiplano of Bolivia. *Palaeogeography, Palaeoclimatology, Palaeoecology, 172*, 269–282.

Frihy, O. E., Deabes, E. A., Abudia, A. A., & Adawi, A. (2022). Heavy mineral composition and texture of the recently formed fluvial delta sediment of Lake Nasser/Nubia, Egypt and Sudan. *International Journal of Sediment Research, 37*, 70–82.

Fügenschuh, B., & Schmid, S. M. (2005). Age and significance of core complex formation in a very curved orogen: Evidence from fission track studies in the South Carpathians (Romania). *Tectonophysics, 404*, 33—53.

Gaigalas, A., Pazdur, A., Michczynski, A., Pawlyta, J., Kleišmantas, A., Melešytė, … Vainorius, J. (2013). Peculiarities of sedimentation conditions in the oxbow lakes of Dubysa River (Lithuania). *Geochronometria, 40*, 22—32.

Gheith, A., Al-Balushi, A., Hereher, M., Sherief, Y., & Al-Awadhi, T. (2021). Petrography and heavy minerals analysis for recognition of the depositional history of the Wahiba Sand Sea, Sultanate of Oman. *Arabian Journal of Geosciences, 14*, 1444.

Giraudi, C. (2014). Coarse sediments in Northern Apennine peat bogs and lakes: New data for the record of Holocene alluvial phases in peninsular Italy. *The Holocene, 24*, 932—943.

Grba, N., Neubauer, F., Šajnović, A., Stojanović, K., & Jovančićević, B. (2015). Heavy metals in Neogene sedimentary rocks as a potential geogenic hazard for sediment, soil, surface, and groundwater contamination (Eastern Posavina and Lopare Basin, Bosnia and Herzegovina). *Journal of the Serbian Chemical Society, 80*, 827—838.

Grba, N., Šajnović, A., Stojanović, K., Simić, V., Jovančićević, B., Roglić, G., & Erić, V. (2014). Preservation of diagenetic products of β-carotene in sedimentary rocks from the Lopare Basin (Bosnia and Herzegovina). *Chemie der Erde, 74*, 107—123.

Grice, K., Schouten, S., Nissenbaum, A., Charrach, J., & Sinninghe Damsté, J. S. (1998). Isotopically heavy carbon in the C21 to C25 regular isoprenoids in halite-rich deposits from the Sdom Formation, Dead Sea Basin. Israel. *Organic Geochemistry, 28*, 349—359.

Hakimi, M. H., Najaf, A. A., Abdula, R. A., & Mohialdeen, I. M. J. (2018). Generation and expulsion history of oil-source rock (Middle Jurassic Sargelu Formation) in the Kurdistan of north Iraq, Zagros folded belt: Implications from 1D basin modeling study. *Journal of Petroleum Science and Engineering, 162*, 852—872.

Harzhauser, M., & Mandić, O. (2008). Neogene lake systems of Central and South-Eastern Europe: Faunal diversity, gradients and interrelations. *Palaeogeography, Palaeoclimatology, Palaeoecology, 260*, 417—434.

Jiamo, F., Guojyng, S., Jiayou, X., Eglinton, G., Gowar, A. P., Rongfren, J., … Pingan, P. (1990). Application of biological markers in the assessment of paleoenvironments of Chinese non-marine sediments. *Organic Geochemistry, 16*, 769—779.

Jiang, Z., & Fowler, M. G. (1986). Carotenoid-derived alkanes in oils from northwestern China. *Organic Geochemistry, 10*, 831—839.

Jordan, T., Quezada, A., Blanco, N., Jensen, A., Vásquez, P., & Sepúlveda, F. (2022). Paleoenvironmental evolution of a Forearc in response to forcings by drainage, climate, volcanism, and tectonics: The Quillagua Depocenter, Chile. *Lithosphere, 1*, 1024844.

Katz, B., & Lin, F. (2014). Lacustrine basin unconventional resource plays: Key differences. *Marine and Petroleum Geology, 56*, 255—265.

Konta, J. (1969). Quantitative analytical petrological classification of sedimentary rocks. *Acta Universitatis Carolinae: Geologica, 3*, 175—253.

Kováč, M., Márton, E., Klučiar, T., & Vojtko, R. (2018). Miocene basin opening in relation to the north-eastward tectonic extrusion of the ALCAPA Mega-Unit. *Geologica Carpathica, 69*, 254—263.

Larcher, A. V., Alexander, R., & Kagi, R. I. (1987). Changes in configuration of extended moretanes with increasing sediment maturity. *Organic Geochemistry, 11*, 59—63.

Lazarević, Z., Milovanović, L., Milivojević, J., & Vasiljević, I. (2019). Palaeoflora of Kamenica (Pranjani Basin, western Serbia). *Geoloski anali Balkanskoga poluostrva, 80*, 53—63.

Leventhal, J. S. (1987). Carbon and sulfur relationship in Devonian shales from the Appalachian Basin as an indicator of environment of deposition. *American Journal of Science, 287*, 33—49.

Lone, A., Fousiya, A. L., Rayees Shah, A. A., & Achyuthan, H. (2018). Reconstruction of paleoclimate and environmental fluctuations since the early Holocene period using organic matter and C:N proxy records: A review. *Journal of the Geological Society of India, 91*, 209—214.

Lukács, R., Harangi, S., Gal, P., Szepesi, J., Di Capua, A., & Fodor, L. (2022). Formal definition and description of lithostratigraphic units related to the Miocene silicic pyroclastic rocks outcropping in Northern Hungary: A revision. *Geologica Carpathica, 73*, 137—158.

Lukács, R., Harangi, S., Guillong, M., Bachmann, O., Fodor, L., Buret, Y., … Zimmerer, M. (2018). Early to Mid-Miocene syn-extensional massive silicic volcanism in the Pannonian Basin (East-Central Europe): Eruption chronology, correlation potential and geodynamic implications. *Earth-Science Reviews, 179*, 1—19.

Lužar-Oberiter, B., Mikes, T., von Eynatten, H., & Babić, L. (2009). Ophiolitic detritus in Cretaceous clastic formations of the Dinarides (NW Croatia): Evidence from Cr-spinel chemistry. *International Journal of Earth Sciences, 98*, 1097—1108.

Malešević, M., Vukanović, M., Obradinović, Z., Dimitrijević, M., Brković, T., Stefanović, M., … Pavlović, Z. (1974). *Explanation to the basic geologic map of Serbia, section K34-31 (Kuršumlija)*. Belgrade: Serbia, Federal Geological Survey. http://geoliss.mre.gov.rs/OGK/RasterSrbija/. (Accessed 10 April 2021). *(In Serbian)*

Mandić, O., de Leeuw, A., Vuković, B., Krijgsman, W., Harzhauser, M., & Kuiper, K. F. (2011). Palaeoenvironmental evolution of Lake Gacko (Southern Bosnia and Herzegovina): Impact of the Middle Miocene Climatic Optimum on the Dinaride Lake System. *Palaeogeography, Palaeoclimatology, Palaeoecology, 299*, 475—492.

Mandić, O., Hajek-Tadesse, V., Bakrač, K., Reichenbacher, B., Grizelj, A., & Miknić, M. (2019c). Multiproxy reconstruction of the middle Miocene Požegapalaeolake in the Southern Pannonian Basin (NE Croatia) prior to the Badenian transgression of the Central Paratethys Sea. *Palaeogeography, Palaeoclimatology, Palaeoecology, 516*, 203—219.

Mandić, O., Rundić, L., Ćorić, S., Pezelj, Đ., Theobalt, D., Sant, K., & Krijgsman, W. (2019a). Age and mode of the middle miocene marine flooding of the pannonianbasin—Constraints from Central Serbia. *PALAIOS, 34*, 71—95.

Mandić, O., Sant, K., Kallanxhi, M. E., Ćorić, S., Theobalt, D., Grunert, P., … Krijgsman, W. (2019b). Integrated bio-magnetostratigraphy of the Badenian reference section Ugljevik in southern Pannonian Basin-implications for the Paratethys history (middle Miocene, Central Europe). *Global and Planetary Change, 172*, 374—395.

Marić, D., Srećković-Batoćanin, D., Vasić, N., Radisavljević, M., & Đekić, T. (2019a). History of the Belanovica (Serbia) Neogene lake basin inferred from petrological and geochemical data. *Geologia Croatica, 1*, 5—18.

Marić, D., Srećković-Batoćanin, D., Vasić, N., Radisavljević, M., & Đekić, T. (2019b). History of the Belanovica (Serbia) Neogene lake basin inferred from petrological and geochemical data. *Geologia Croatica, 72*, 5—18.

Marinović, Đ., & Rundić, L. (2020). Depth geological relations of the wider area of Belgrade-based on the wells and geophysical data. *Geoloski anali Balkanskoga poluostrva, 81*(2), 1—32.

Marović, M., Đoković, I., Pešić, L., Radovanović, S., Toljić, M., & Gerzina, N. (2002). Neotectonics and seismicity of the southern margin of the Pannonian basin in Serbia. *European Geoscience Union, Stephan Mueller Special Publication Series, 3*, 277—295.

Marović, M., Đoković, I., Toljić, M., Milivojević, J., & Spahić, D. (2007a). Paleogene-early miocene deformations of Bukulja-Venčac crystalline (Vardar zone, Serbia). *Geološki anali Balkanskoga poluostrva, 68*, 9—20.

Marović, M., Đoković, I., Toljić, M., Spahić, D., & Milivojević, J. (2007b). Extensional unroofing of the Veliki Jastrebac dome (Serbia). *Geološki anali Balkanskoga poluostrva, 68*, 21—27.

Marović, M., Mihailović, D., Đoković, I., Gerzina, N., & Toljić, M. (2001). Wrench tectonics of the Paleogene—Lower Miocene basins of Serbia between the central part of the Vardar Zone and the Moesian Plate. In *September 19—23, 2001, Sopron, Hungary. Proceedings, Pancardi 2001 Meeting*. p. DP-9.

Marović, M., Toljić, M., Rundić, L., & Milivojević, J. (2007c). *Neoalpine tectonics of Serbia*. Belgrade, Serbia: Serbian Geological Society.

Matenco, L., & Radivojević, D. (2012). On the formation and evolution of the Pannonian Basin: Constraints derived from the structure of the junction area between the Carpathians and Dinarides. *Tectonics, 31*, TC6007.

Menant, A., Jolivet, L., & Vrielynck, B. (2016). Kinematic reconstructions and magmatic evolution illuminating crustal and mantle dynamics of the eastern Mediterranean region since the late Cretaceous. *Tectonophysics, 675*, 103—140.

Meulenkamp, J. E., & Sissingh, W. (2003). Tertiary palaeogeography and tectonostratigraphic evolution of the Northern and Southern Peri-Tethys platforms and the intermediate domains of the African—Eurasian convergent plate boundary zone. *Palaeogeography, Palaeoclimatology, Palaeoecology, 196*(1—2), 209—228.

Meyers, P., & Ishiwatari, R. (1993). Lacustrine organic geochemistry — An overview of indicators of organic matter sources and diagenesis in lake sediments. *Organic Geochemistry, 20*, 867—900.

Meyers, P., & Lallier-Vergès, E. (1999). Lacustrine sedimentary organic matter records of Late Quaternary paleoclimates. *Journal of Paleolimnology, 21*, 345—372.

NCS FC 28009L. (2016). *Certificate of certified reference material, coal*. Beijing, China: China National Analysis Center for Iron and Steel.

Nováková, P., Rybar, S., Šarinová, K., Nagy, A., Hudáčková, N., Jamrich, M., … Kováč, M. (2020). The late Badenian-Sarmatian (Serravallian) environmental transition calibrated by sequence stratigraphy (eastern Danube Basin, Central Paratethys). *Geologica Carpathica, 71*, 291—313.

Obradović, J., & Vasić, N. (2007). *Neogene lacustrine basins of Serbia*. Belgrade, Serbia: Serbian Academy Sciences et Arts, Monographs 662, Department of Mathematics, Physics and Geo Sciences. *(in Serbian,with English summary)*

Olgun, N., Duggen, S., Andronico, D., Kutterolf, S., Croot, P. L., Giammanco, S., … Randazzo, L. (2013). Possible impacts of volcanic ash emissions of Mount Etna on the primary productivity in the oligotrophic Mediterranean Sea: Results from nutrient release experiments in seawater. *Marine Chemistry, 152*, 32—42.

Orkhonselenge, A., Uuganzaya, M., & Davaagatan, T. (2022). Formation and evolution of lakes in Mongolia. In *Lakes of Mongolia. Lakes of Mongolia. Syntheses of Limnogeology*. Berlin: Springer International Publishing.

OXSAS. (2013). *OXSAS™ optical emission analytical software*. Waltham, MA, U.S.: Thermo Fisher Scientific Inc. http://www.thermoscientific.com/content/dam/tfs/ATG/CAD/CAD%20Documents/Product%20Manulas%20&%20Specifications/Elemental%20Analysis/XRF/XR-PS41141-OXSAS%20XRF-Hi-9713.pdf. (Accessed 17 May 2021).

Peshkov, G. A., Chekhonin, E. M., Rüpke, L. H., Musikhin, K. A., Bogdanov, O. A., & Myasnikov, A. V. (2021). Impact of differing heat flow solutions on hydrocarbon generation predictions: A case study from West Siberian Basin. *Marine and Petroleum Geology, 124*, 104807.

Peters, K. E., & Moldowan, J. M. (1991). Effects of source, thermal maturity, and biodegradation on the distribution and isomerization of homohopanes in petroleum. *Organic Geochemistry, 17*, 47—61.

Pezelj, Đ., Mandić, O., & Ćorić, S. (2013). Paleoenvironmental dynamics in the southern Pannonian Basin during initial Middle Miocene marine flooding. *Geologica Carpathica, 64*, 81—100.

Pujos, M., Bouysse, P., & Pons, J.-C. (1990). Sources and distribution of heavy minerals in late quaternary sediments of the French Guiana continental shelf. *Continental Shelf Research, 10*, 59–79.

Radivojević, D. (2023). Evolution of the southeastern part of the Pannonian Basin and its implications. *Geoloski anali Balkanskoga poluostrva, 84*, 133–145.

Reading, H. G. (2009). *Sedimentary environments: Processes, facies and stratigraphy*. Hoboken, NJ, U.S: John Wiley & Sons.

Rundić, L. (2022). Ostracods as indicator of the badenian marine flooding (Central Parathetys, Bosnia & Herzegovina and Serbia). *Journal of Faculty of Mining, Geology and Civil Engineering, 1*, 49–50.

Rundić, L., Knežević, S., & Rakijaš, M. (2013). Middle Miocenebadenian transgression: New evidences from the Vrdnik coal basin (Fruška Gora Mt., Northern Serbia). *Geoloski anali Balkanskoga poluostrva, 74*, 9–23.

Rybár, S., Halásová, E., Hudáčková, N., Kováč, M., Kováčová, M., Šarinová, K., & Šujan, M. (2015). Biostratigraphy, sedimentology and paleoenvironments of the northern Danube Basin: Ratkovce 1 well case study. *Geologica Carpathica, 66*, 51–67.

Rybár, S., & Kotulová, J. (2023). Petroleum play types and source rocks in the Pannonian basin, insight from the Slovak part of the Danube Basin. *Marine and Petroleum Geology, 149*, 106092.

Rybar, S., Kováč, M., Sarinová, K., Halasova, E., Hudáčková, N., Šujan, M., … Klučiar, T. (2016). Neogene changes in palaeogeography, palaeoenvironment, and the provenance of sediment in the Northern Danube Basin. *Bulletin of Geosciences, 91*, 367–398.

Šajnović, A., Grba, N., Neubauer, F., Kašanin-Grubin, M., Stojanović, K., Petković, N., & Jovančićević, B. (2020). Geochemistry of sediments from the Lopare Basin (Bosnia and Herzegovina): Implications for paleoclimate, paleosalinity, paleoredox and provenance. *Acta Geologica Sinica-English Edition, 94*, 1591–1618.

Šajnović, A., Simić, V., Jovančićević, B., Cvetković, O., Dimitrijević, R., & Grubin, N. (2008). Sedimentation history of neogene lacustrine sediments of Sušeočka Bela Stena based on geochemical parameters (Valjevo-Mionica Basin, Serbia). *Acta Geologica Sinica-English Edition, 82*, 1201–1212.

Salama, W., Anand, R. R., & Verrall, M. (2016). Mineral exploration and basement mapping in areas of deep transported cover using indicator heavy minerals and paleoredox fronts, Yilgarn Craton, Western Australia. *Ore Geology Reviews, 72*, 485–509.

Sandiford, A., Alloway, B., & Shane, P. (2001). A 28 000–6600 cal yr record of local and distal volcanism preserved in a paleolake, Auckland, New Zealand. *New Zealand Journal of Geology and Geophysics, 44*, 323–326.

Sant, K., Kuiper, K. F., Rybar, S., Grunert, P., Harzhauser, M., Mandic, O., … Krijgsman, W. (2020). 40Ar/39Ar geochronology using high sensitivity mass spectrometry: Examples from middle Miocene horizons of the Central Paratethys. *Geologica Carpathica, 71*, 166–182.

Šarinová, K., Escamilla, J., Jourdan, F., Frew, A., Mayers, C., Kováčová, … Kováč, M. (2021a). 40Ar/39Ar geochronology of Burdigalian paleobotanical localities in the central Paratethys (south Slovakia). *Geológica Acta, 19*, 6.

Šarinová, K., Hudáčková, N., Rybár, S., Jamrich, M., Jourdan, F., Frew, A., … Sliva, Ľ. (2021b). 40 Ar/39 Ar dating and palaeoenvironments at the boundary of the early-late Badenian (Langhian-Serravallian) in the northwest margin of the Pannonian basin system. *Facies, 67*, 1–27.

Šarinová, K., Rybár, S., Halásová, E., Hudáčková, N., Jamrich, M., Kováčová, M., & Šujan, M. (2018). Integrated biostratigraphical, sedimentological and provenance analyses with implications for lithostratigraphic ranking: The Miocene Komjatice depression of the Danube Basin. *Geologica Carpathica, 69*, 382–409.

Schmid, M. S., Bernoulli, D., Fügenschuh, B., Matenco, L., Schefer, S., Schuster, R., … Ustaszewski, K. (2008). The Alps-Carpathians-Dinarides-connection: A correlation of tectonic units. *Swiss Journal of Geosciences, 101*, 139–183.

Schmid, M. S., Fügenschuh, B., Kounov, A., Matenco, L., Nievergelte, P., Oberhänsli, R., … van Hinsbergen, D. J. J. (2020). Tectonic units of the Alpine collision zone between Eastern Alps and western Turkey. *Gondwana Research, 78*, 308–374.

Scott, J. J., Buatois, L. A., & Mangano, M. G. (2012). Lacustrine environments. In *Developments in sedimentology* (Vol. 64, pp. 379–417). Amsterdam, TheNetherlands: Elsevier.

Seifert, W. K., & Moldowan, J. M. (1980). The effect of thermal stress on source-rock quality as measured by hopane stereochemistry. *Physics and Chemistry of the Earth, 12*, 229–237.

Sinninghe Damasté, J. S., Keing, F., Koopmans, M. F., Koster, J., Schouten, S., Hayes, J. M., & de Leeuw, J. W. (1995). Evidence for gammacerane as an indicator of water column stratification. *Geochimica et Cosmochimica Acta, 59*, 1895–1900.

Spahić, D. (2006). *Geological setting of the Veliki Jastrebac Mt. (central Serbia)* (Magister's dissertation). Geological Survey of Serbia, https://doi.org/10.13140/RG.2.2.30882.50884. Retrieved from: https://www.researchgate.net/ publication/366372503_Geological_setting_of_the_Veliki_Jastrebac_Mt_central_ Serbia. *(in Serbian)*

Spahić, D. (2022a). Remarks on the Oligo-Miocene extensional episode (s) in Inner Dinarides: Towards the tectonic constraints of the origin of intra-montagne basins. *Geološki anali Balkanskoga poluostrva, 83*, 39–56.

Spahić, D. (2022b). Towards the Triassic configuration of western Paleotethys. *Journal of Earth Science, 33*, 1494–1512.

Spahić, D., Exner, U., Behm, M., Grasemann, B., Haring, A., & Pretsch, H. (2011). Listric versus planar normal fault geometry: An example from the Eisenstadt-Sopron Basin (E Austria). *International Journal of Earth Sciences, 100*, 1685–1695.

Spahić, D., & Gaudenyi, T. (2019). Intraoceanic subduction model of northwestern Neotethys and geodynamic interaction with Serbo-Macedonian foreland: Descending vs. overriding near-trench dynamic constraints (East Vardar Zone, Jastrebac Mts., Serbia). *Geološki anali Balkanskoga poluostrva, 80*, 65–85.

Spahić, D., & Gaudenyi, T. (2020). The role of the 'Zvornik suture' for assessing the number of Neotethyan oceans: Surface-subsurface constraints on the fossil plate margin (Vardar Zone vs. Inner Dinarides). *Geološki anali Balkanskoga poluostrva, 81*, 63–86.

Spahić, D., & Gaudenyi, T. (2022). On the Sava Suture Zone: Post-Neotethyan oblique subduction and the origin of the Late Cretaceous mini-magma pools. *Cretaceous Research, 131*, 105062.

Spahić, D., Grasemann, B., & Exner, U. (2013). Identifying fault segments from 3D fault drag analysis (Vienna Basin, Austria). *Journal of Structural Geology, 55*, 182–195.

Spahić, D., Šajnović, A., Burazer, N., Radisavljević, M., & Jovančićević, B. (2023). Neogene subsidence rates of the southern Peri Pannonian Realm (1D basin modeling): Constraints on the extensional geodynamic drivers of the asymmetric Toplica Basin (central-southern Serbia). *Geoenergy Science and Engineering, 226*, 211714.

Spencer, J. E. (2006). *A geologist's guide to the core complex geology along the Catalina Highway, Tucson area, Arizona. Arizona Geological Survey Open File Report 06-01 version 1.1*. Tucson, AZ, U.S.: Arizona Geological Survey.

STSD-3. (1990). *Stream Sediments Reference Materials STSD-1 to STSD-4, Stream Sediment*. Ontario, Canada: CANMET Mining and Mineral Science Laboratories.

Subová, V., Rybár, S., Šarinová, K., Hudáčková, N., Jamrich, M., Sliva, Ľ., … Hlavatý, I. (2022). Evolution of the lower Badenian depositional system in the East Slovakian Basin: Implications for reservoir rock potential. *Geologica Carpathica, 73*, 319–352.

Tari, G., Bada, G., Beindinger, A., Csizmeg, J., Danišik, M., Gjerazi, I., … Szafián, Ð. (2021). The connection between the Alps and the Carpathians beneath the Pannonian Basin: Selective reactivation of Alpine nappe contacts during Miocene extension. *Global and Planetary Change, 197*, 103401.

Tari, G. C., Gjerazi, I., & Grasemann, B. (2020). Interpretation of vintage 2D seismic reflection data along the Austrian-Hungarian border: Subsurface expression of the Rechnitz metamorphic core complex. *Interpretation, 8*, SQ73–SQ91.

Uematsu, M., Toratani, M., Kajino, M., Yasushi Narita, Y., Senga, Y., & Kimoto, T. (2004). Enhancement of primary productivity in the western North Pacific caused by the eruption of the Miyake-jima Volcano. *Geophysical Research Letters, 31*, L06106.

UniQuant. (2015). Waltham, MA, USA: Thermo Fisher Scientific Inc. http://www.uniquant.com. (Accessed 17 May 2021).

Valero-Garcés, B., Morellón, M., Moreno, A., Corella, J. P., Martin-Puertas, C., Barreiro, F., … Mata-Campo, M. P. (2014). Lacustrine carbonates of Iberian Karst Lakes: Sources, processes and depositional environments. *Sedimentary Geology, 299*, 1–9.

Vlček, T., Kováčová, M., Šarinová, K., Rybár, S., Hudáčková, N., Ruman, A., … Franců, J. (2022). Multiproxy constraints on Central Parathethys Sea and Lake Pannon paleoclimate and paleoenvironment transitions during the Middle-Late Miocene (Danube Basin, Slovakia). *Palaeogeography, Palaeoclimatology, Palaeoecology, 600*, 111058.

Vlček, T., Šarinová, K., Rybár, S., Hudáčková, N., Jamrich, M., Šujan, M., … Kováčová, M. (2020). Paleoenvironmental evolution of Central Parathethys Sea and Lake Pannon during the Cenozoic. *Palaeogeography, Palaeoclimatology, Palaeoecology, 559*, 109892.

Wilkin, R. T., & Barnes, H. L. (1996). Formation processes of framboidal pyrite. *Geochimica et Cosmochimica Acta, 61*, 323–339.

Zatoň, M., Rakociñski, M., & Marynowski, L. (2008). Pyrite framboids as paleoenvironmental indicators. *Przegld Geologiczny, 56*, 158–164. *(In Polish)*